AD/A-004 002

MODIFIED CENTRIFUGAL COMPRESSOR

Gary B. Reeves, et al

Pratt and Whitney Aircraft

Prepared for:

Army Air Mobility Research and Development Laboratory

November 1974

UNCLASSIFIED

SECURITY CLASSIFICATION OF THIS PAGE *(When Data Entered)*

REPORT DOCUMENTATION PAGE		READ INSTRUCTIONS BEFORE COMPLETING FORM
1. REPORT NUMBER USAAMRDL-TR-74-96	2. GOVT ACCESSION NO.	3. RECIPIENT'S CATALOG NUMBER AD/A-004002
4. TITLE *(and Subtitle)* MODIFIED CENTRIFUGAL COMPRESSOR		5. TYPE OF REPORT & PERIOD COVERED Final 23 October 1973 to 23 July 1974
		6. PERFORMING ORG. REPORT NUMBER FR-6583
7. AUTHOR(s) Gary B. Reeves, Jeffrey K. Schweitzer		8. CONTRACT OR GRANT NUMBER(s) DAAJ02-74-C-0003
9. PERFORMING ORGANIZATION NAME AND ADDRESS Pratt & Whitney Aircraft Division/United Aircraft Corporation/Florida Research and Development Center West Palm Beach, Florida 33402		10. PROGRAM ELEMENT, PROJECT, TASK AREA & WORK UNIT NUMBERS Task 1G262207AH8901
11. CONTROLLING OFFICE NAME AND ADDRESS Eustis Directorate/U.S. Army Air Mobility Research and Development Laboratory Fort Eustis, Virginia 23604		12. REPORT DATE November 1974 13. NUMBER OF PAGES 82
14. MONITORING AGENCY NAME & ADDRESS*(if different from Controlling Office)*		15. SECURITY CLASS. *(of this report)* Unclassified 15a. DECLASSIFICATION/DOWNGRADING SCHEDULE

16. DISTRIBUTION STATEMENT *(of this Report)*

Approved for public release; distribution unlimited.

17. DISTRIBUTION STATEMENT *(of the abstract entered in Block 20, if different from Report)*

18. SUPPLEMENTARY NOTES

19. KEY WORDS *(Continue on reverse side if necessary and identify by block number)*

Centrifugal Compressor
Inducer
Diffuser
Performance
Impeller

20. ABSTRACT *(Continue on reverse side if necessary and identify by block number)*

A single-stage centrifugal compressor designed to produce a 10:1 pressure ratio at a flow rate of 3.2 lb/sec was tested. An earlier version of this compressor was tested under USAAMRDL Contract DAAJ02-70-C-0006 and was found to have excessive losses in the tandem inducer. In addition, diffuser damage was incurred during that testing, which also prevented the achievement of the full design potential. The objective of this follow-on program was therefore to demonstrate improved

DD FORM 1 JAN 73 1473 EDITION OF 1 NOV 65 IS OBSOLETE

UNCLASSIFIED

SECURITY CLASSIFICATION OF THIS PAGE *(When Data Entered)*

EUSTIS DIRECTORATE POSITION STATEMENT

The objectives cited in this report are founded in the larger effort of the U. S. Army to improve the effectiveness of propulsion systems for future military applications. The stated performance goals and reported achievements are applicable engine technology which have the potential for providing lighter, more efficient, simpler, and more rugged gas turbine engines than are now in the field. The immediate results are only partially usable, in that the efficiency of the demonstrated compressor peaks at the surge line and any practical engine using this hardware would necessarily operate with some surge margin and at lower-than-peak efficiency.

This report has been reviewed by technical personnel from this Directorate, and the conclusions and recommendations contained herein are concurred in by this Directorate. The project engineer for this contract was Mr. Robert A. Langworthy, Propulsion Technical Area, Technology Applications Division.

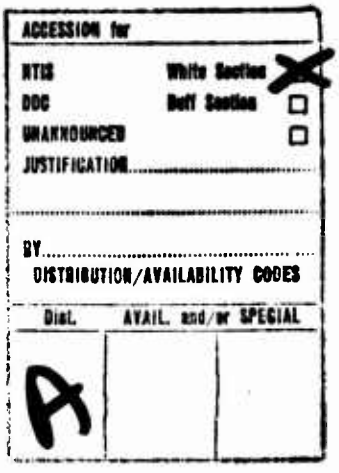

DISCLAIMERS

The findings in this report are not to be construed as an official Department of the Army position unless so designated by other authorized documents.

When Government drawings, specifications, or other data are used for any purpose other than in connection with a definitely related Government procurement operation, the United States Government thereby incurs no responsibility nor any obligation whatsoever; and the fact that the Government may have formulated, furnished, or in any way supplied the said drawings, specifications, or other data is not to be regarded by implication or otherwise as in any manner licensing the holder or any other person or corporation, or conveying any rights or permission, to manufacture, use, or sell any patented invention that may in any way be related thereto.

Trade names cited in this report do not constitute an official endorsement or approval of the use of such commercial hardware or software.

DISPOSITION INSTRUCTIONS

Destroy this report when no longer needed. Do not return it to the originator.

Block 20 (Continued)

performance for the 10:1 pressure ratio single-stage centrifugal compressor with a modified inducer and a new (undamaged) diffuser. Modifications to the design of the inducer were made to improve its high-speed (Mach number) performance and to decrease the required inlet prewhirl, and a test program was conducted to obtain overall and inducer performance data.

A total-to-static pressure ratio of 10.07:1 and a corresponding adiabatic efficiency of 78.4% were recorded at design prewhirl and 99% of design speed. This performance exceeded the original 10:1 pressure ratio single-stage centrifugal compressor goal of 75% by 3.4 points and substantiated the design modification to the inducer and the matching of the diffuser to the improved compressor performance expected to result from the altered inducer. The entire test sequence was conducted at sea level conditions without mechanical difficulty, and all contract data requirements were fulfilled.

The results at this program are applicable to small gas turbine engines. The compressor design centered on this application and included some compromise to permit a front-drive turboshaft configuration. The efficiency demonstrated is comparable to existing small engine compressor performance, but generally at a higher pressure ratio and in a single-stage rather than in a multistage machine.

PREFACE

This report is the Final Technical Report to fulfill the data requirements of Contract DAAJ02-74-C-0003 with the Eustis Directorate, U.S. Army Air Mobility Research and Development Laboratory, Fort Eustis, Virginia.

The principal investigator and Program Manager of this effort was Gary B. Reeves. The U.S. Army Project Engineer was Mr. Robert A. Langworthy, Technology Applications Division. The authors wish to acknowledge Pratt & Whitney personnel E. T. Singleton (Inducer Design), L. L. Coons (Design Coordination), J. K. Schweitzer (Data Reduction and Analysis), and J. D. Goodrum (Assembly and Test) for their participation and contributions to the program and W. J. McAnally, III, for overall and administrative guidance and support.

CONTENTS

ILLUSTRATIONS

ILLUSTRATIONS (Continued)

ILLUSTRATIONS (Continued)

TABLES

SECTION I

INTRODUCTION

The high-pressure-ratio, single-stage centrifugal compressor is a major element in the Army's continuing effort to simplify and improve the performance of gas turbine compressors in the 2-5 lb/sec airflow class. Contract DAAJ02-70-C-0006,[a] hereinafter referred to as the "10:1 program," also with Pratt & Whitney Aircraft, provided for the design and testing of a 10:1 pressure ratio compressor required for future small, advanced gas turbines.

In its "as-designed" configuration, the compressor provided only a 9.34 pressure ratio and its flow rate was 2% less than design; efficiency exceeded the 75% goal, however, by 2 points. The achievement of the 10:1 pressure ratio required an increase in rotor speed of 1% and a reduction of inducer prewhirl from 10 deg to -4 deg. These two changes resulted in higher inducer blade loadings specifically due to higher incidence and relative Mach number; consequently, an inducer efficiency loss of approximately 17.5 points was noted between 95 and 101% rotor speeds, which contributed to an overall efficiency loss of 4 points. An additional loss in overall compressor efficiency was incurred when debris from an impeller-shroud rub damaged the diffuser leading edges. The resulting efficiency at the 10:1 pressure ratio was 1.2 percentage points below the 75% goal.

The objective of this program was to demonstrate the performance potential of the 10:1 centrifugal compressor with an inducer designed to overcome the observed high Mach number losses and a diffuser conforming to the original specification (undamaged).

---

[a] McAnally, W. J., III, 10:1 PRESSURE RATIO SINGLE-STAGE CENTRIFUGAL COMPRESSOR PROGRAM, Pratt & Whitney Aircraft, USAAMRDL Technical Report 74-15, Eustis Directorate, U.S. Army Air Mobility Research and Development Laboratory, Fort Eustis, Virginia, April 1974.

SECTION II

DESIGN

No modifications were made to any of the nonaerodynamic (mechanical) components of the test rig or drive turbine used in the 10:1 program. A summary of modifications to the aerodynamic components is listed in table 1.

TABLE 1. SUMMARY OF AERODYNAMIC COMPONENT MODIFICATIONS

Item	Comment
Bellmouth and Nose Cone	No modification
Inlet Strut Case	No modification except for shortening the hub wall aft of the inlet guide vanes to prevent interference with the modified inducer disk
Inlet Guide Vanes and Inlet Guide Vane Shroud Case	No modification
Inducer	Redesigned to improve efficiency at design speed
Inducer Shroud	Modified to accept redesigned inducer with 0.005-in. nominal design running clearance
Impeller	No modification
Impeller Shroud	No modification
Diffuser	Newly fabricated to correct physical damage and corrosion and rematched with 0.004 in. smaller throat diameter
Exhaust Collector	No modification

INDUCER

The original 10:1 program inducer consisted of multiple circular arc airfoil sections designed for subsonic inducer inlet relative Mach numbers over the inner portion of the span and supersonic inlet relative Mach numbers over the outer portion of the span. However, as the rotor speed was increased and inlet prewhirl decreased from design conditions during the 10:1 program to obtain design compressor pressure ratio, the subsonic sections were subjected to supersonic inlet relative Mach numbers and consequent efficiency deterioration. The inducer was therefore redesigned for this program based on current transonic fan technology to obtain increased pressure ratio and improved efficiency. Specifically, the redesign included: (1) a change in blading distribution to accept higher entrance relative Mach numbers, (2) sizing to accept demonstrated flow rate with 3% choke margin, (3) increasing camber to produce

more work at design flow than the 10:1 program inducer, and (4) a reduction in aspect ratio to improve loading-efficiency characteristics.

The ground rules for the aerodynamic design were (1) no change in flow path to minimize the cost by using as much of the 10:1 program hardware as possible, (2) no change to the variable inlet guide vanes to allow the inducer design to benefit by using loss and turning data generated during the 10:1 program, and (3) no change in air angle out of the inducer since the 10:1 program impeller performance was adequate with these entrance conditions. The 10:1 program flow path was maintained, but approximately 0.3 inch of the available axial space in the vicinity of the inducer was used to lower the aspect ratio of the blade, as shown in Figure 1.

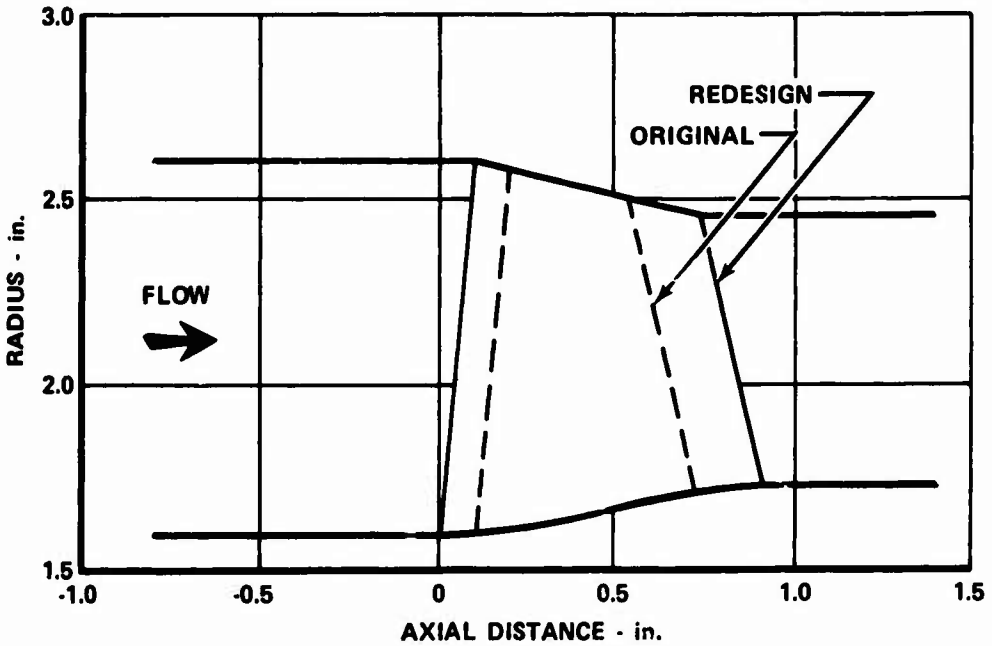

Figure 1. Inducer Modifications.

The modified inducer is comprised of multiple circular arc airfoil (MCA) sections designed on conical surfaces that approximate stream surfaces. Airfoil sections are defined by specifying total and front chord, total and front camber, maximum thickness and its location, stagger, and leading- and trailing-edge radii. Figure 2 shows a schematic drawing of an MCA airfoil with the appropriate nomenclature.

Using the velocity triangle information from a streamline analysis computer program, the blade shape was optimized to minimize the normal shock loss while maintaining sufficient margin to prevent choking in the blade passage. This optimization was carried out by varying front chord and location of maximum thickness and iterating to $A/A^* = 1.03$. The shock strength and losses increase as the location of maximum thickness is moved toward the trailing edge of the blade. The optimum location of maximum thickness is at 60% of the chord, and the optimum front chord is 50% of the total chord. The solidity was selected after several iterations on chord and tip solidity. The tip solidity of 1.52 is based on 18 blades and was selected to keep the blade loadings reasonably low.

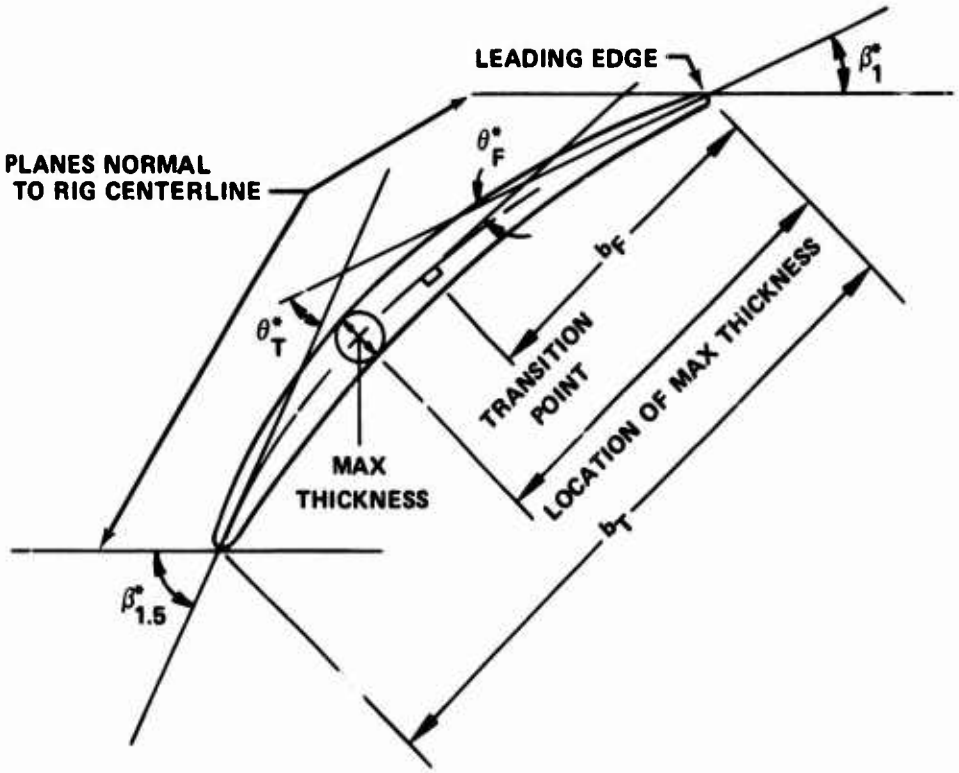

Figure 2. Multiple Circular Arc Airfoil Definitions.

The inducer was designed to operate with the variable inlet guide vanes in the 0-deg swirl position, which produced lowest inlet guide vane losses. Total pressure and air angle profiles from test results obtained during the 10:1 program were used in the design analysis.

The incidence for the supersonic sections was set approximately 1.75 deg to a point on the suction surface halfway between the leading edge and the first captured Mach wave emanation point. The incidence was selected based on a correlation with the LER-to-r ratio that has been successfully used in previous Pratt & Whitney axial compressor designs. Incidence for the subsonic section was selected based on P&WA cascade data for circular arc airfoils.

The profile loss was calculated based on a P&WA correlation of loss parameter vs diffusion factor. The model selected had been successfully used in the design of a 1600-ft/sec stage[b] and was derived from data from three engine compressors and two NASA contract compressors. The deviation angles were based on a modified Carters rule, with an experience factor based on test results of a 1600-ft/sec stage test with a design pressure ratio of 2.00:1.

The design of the modified inducer is summarized in Figure 3. Pertinent information on the design point of the modified inducer and the original 10:1 inducer is shown in Table 2.

---

[b]Monsarrat, N. T., Keenan, M. J., and Tramm, P. C., DESIGN REPORT, SINGLE-STAGE EVALUATION OF HIGHLY-LOADED HIGH-MACH-NUMBER COMPRESSOR STAGES, NASA CR-72562, NASA LEWIS RESEARCH CENTER, Cleveland, Ohio, July 1969.

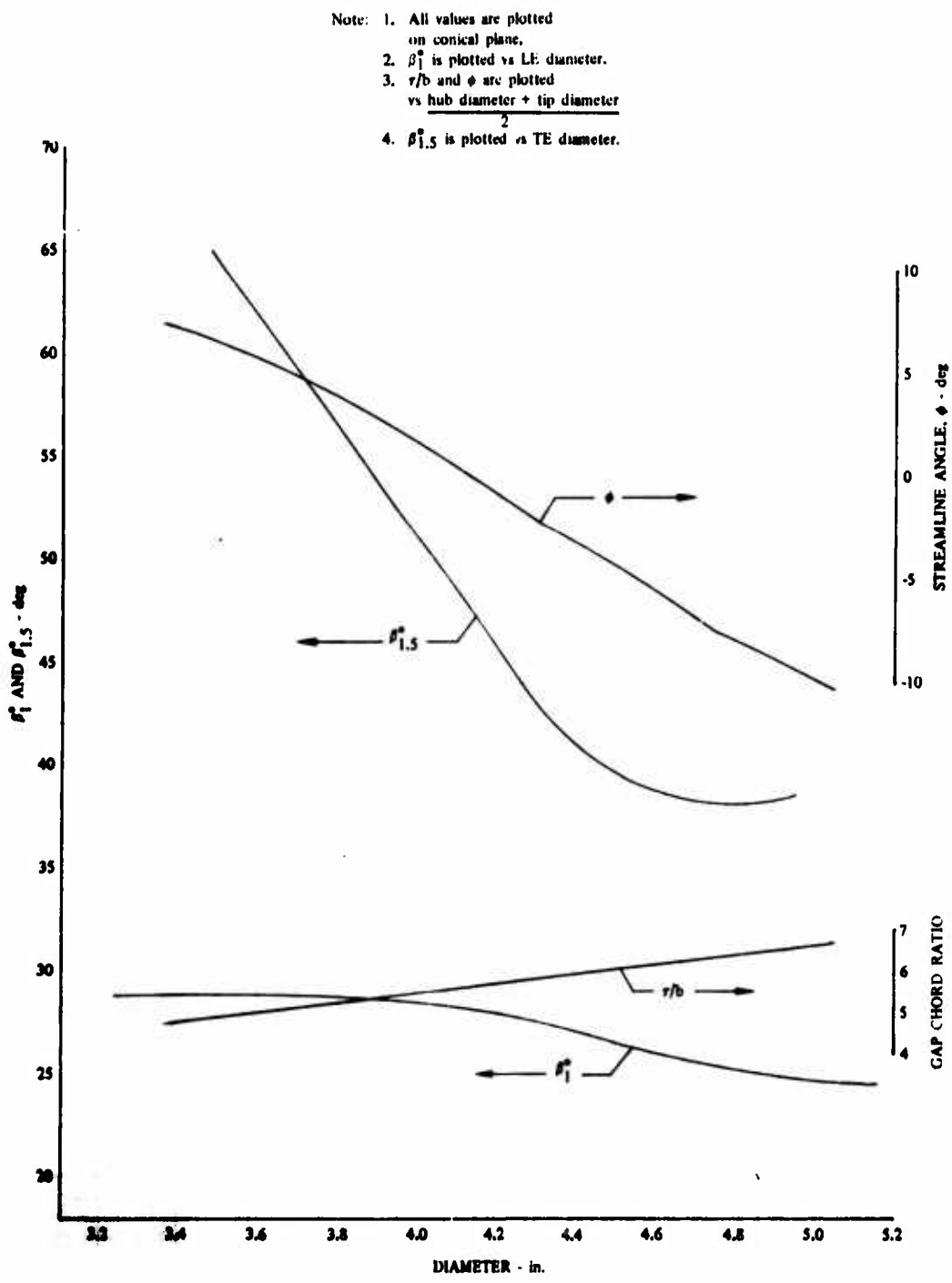

Figure 3. Modified Inducer Design; Low Aspect Ratio and High Solidity. (Sheet 1 of 2)

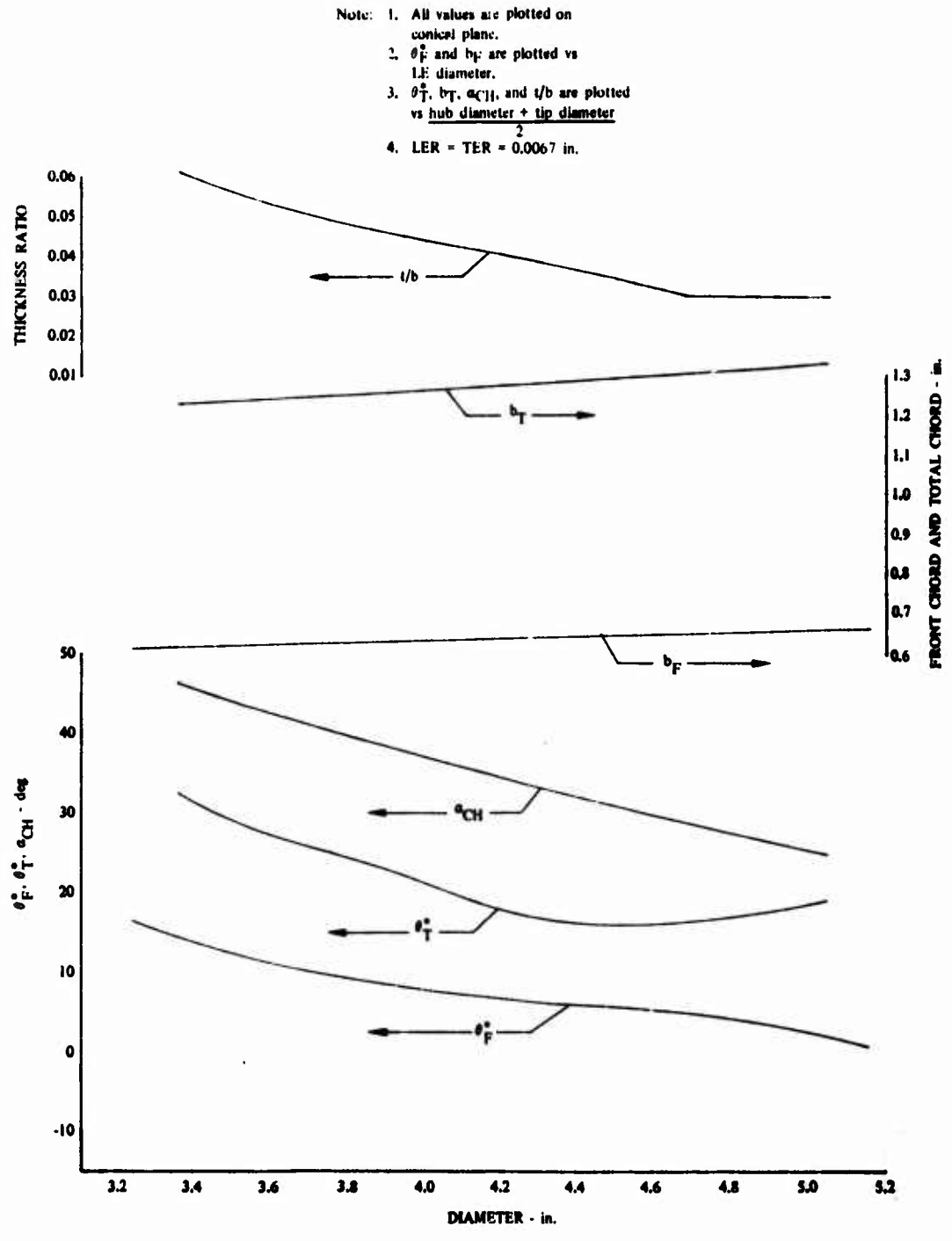

Figure 3. Modified Inducer Design; Low Aspect Ratio and High Solidity. (Sheet 2 of 2)

TABLE 2. INDUCER AERODYNAMIC DESIGN POINT INFORMATION

	Modified Inducer		10:1 Inducer	
Corrected Speed, rpm	65,300		65,300	
Corrected Flow, lb_m/sec	3.2		3.1	
Inducer Pressure Ratio	1.924		1.57	
Inducer Adiabatic Efficiency, %	92		87.6	
Aspect Ratio $\left(= \frac{\text{Mean Span}}{\text{Tip Chord}} \right)$	0.644		1.04	
Number of Blades	18		24	
Inducer Inlet Hub-Tip Ratio	0.615		0.615	
Inducer Tip Speed, ft/sec	1,470		1,470	
Design Prewhirl, deg	0		10	
Inducer Inlet Tip Relative Mach Number	1.43		1.354	
	Hub	Tip	Hub	Tip
Chord, in.	1.23	1.33	0.826	0.826
Inducer Diffusion Factor	0.519	0.487	0.3909	0.3985
Solidity	2.11	1.52	1.92	1.25
Thickness Ratio	0.06	0.03	0.090	0.038

The modified inducer and disk were structurally analyzed using a finite element analysis computer program. Four situations were analyzed to study the interactive effects of the loads resulting from interference fits at the interfaces of joining parts on inducer stress. They included: axial load only, axial load plus radial load due to inner tiebolt, axial load plus radial load due to impeller, and the final case of all loads applied simultaneously. From these cases, the running fits and loads were determined once the assembly fit was specified. A stress summary is shown in Table 3 that indicates both the magnitude and location of the maximum effective stress. The analysis reveals a burst margin of 58% and a maximum effective stress of 80.3 ksi for the material chosen, PWA 1216 (6-2-4-6 titanium). This material has a 0.2% yield stress of 135 ksi, thus indicating a substantial margin of strength relative to the peak effective stress.

TABLE 3. MODIFIED INDUCER STRESS SUMMARY

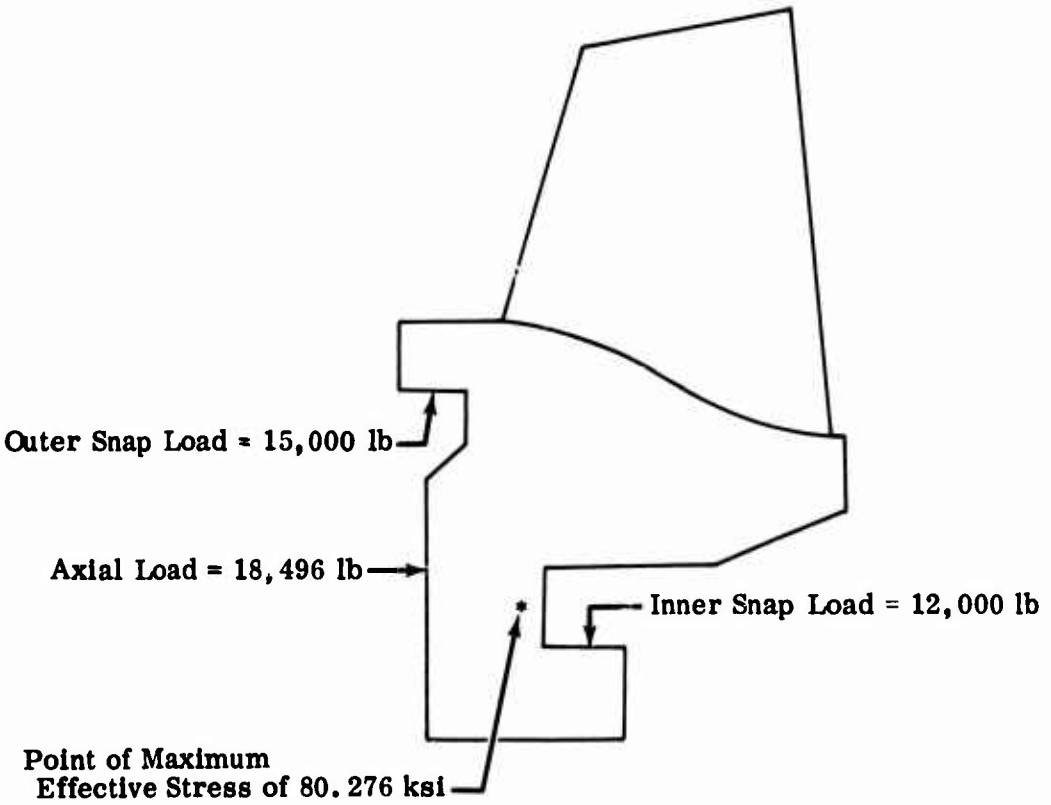

Material:	PWA 1216
Temperature:	200°F
Ultimate Tensile Stress:	159 ksi
0.2% Yield Stress:	135 ksi
Coefficient of Thermal Expansion:	4.78×10^{-6} in./in.
Elastic Modulus:	16.1×10^{6} psi
Operating Speed:	65,300 rpm
Blade Pull:	23,139 lb
Material Utilization Factor:	0.75
Average Tangential Stress:	47.68 ksi
Burst Margin:	1.58
Maximum Effective Stress:	80.276 ksi at point*

Analytical resonance predictions were made for the modified inducer and were adjusted to reflect the differences between the predicted and measured natural frequencies of the original 10:1 program inducer. The measured natural frequencies are shown as reconstructed time-average holograms in Figure 4. The adjustment is based on the similarity of analysis techniques and component configuration. The predicted and measured vibrational characteristics are shown in Figure 5. The inducer was analyzed as a cantilevered airfoil with a constant cross section.

The analysis shows that the modified inducer with a 3% thickness/chord at the tip has no critical resonance modes predicted. The potential for a vibrational failure is also greatly reduced by the low steady-state stresses in the airfoil. The maximum steady-state stress is 31 ksi at the trailing edge of the airfoil root, which is only 21% of the allowable stress and results in a fatigue strength of approximately 60 ksi.

DIFFUSER

The diffuser design for the rotor with the new inducer is shown in Figure 6. All of the basic design features of the 10:1 program diffuser are maintained with the exception of a reduction in diffuser throat diameter from 0.235 to 0.230 to 0.231 in., reflecting the improved performance expected from the redesigned inducer. The diffuser design features the same tangency radius as the 10:1 program diffuser, a 3-deg to 5-deg double cone diffusing passage, a throat length equal to the throat radius, and an overall area ratio of approximately 3.5. The diffuser material was also changed from 410 stainless to AM 355 to prevent the corrosion that had had detrimental effects on performance during the 10:1 program. The AM 355 material was selected over several other corrosion-resistant materials because of the high-temperature requirements and the necessity to obtain similar expansion characteristics with adjacent materials.

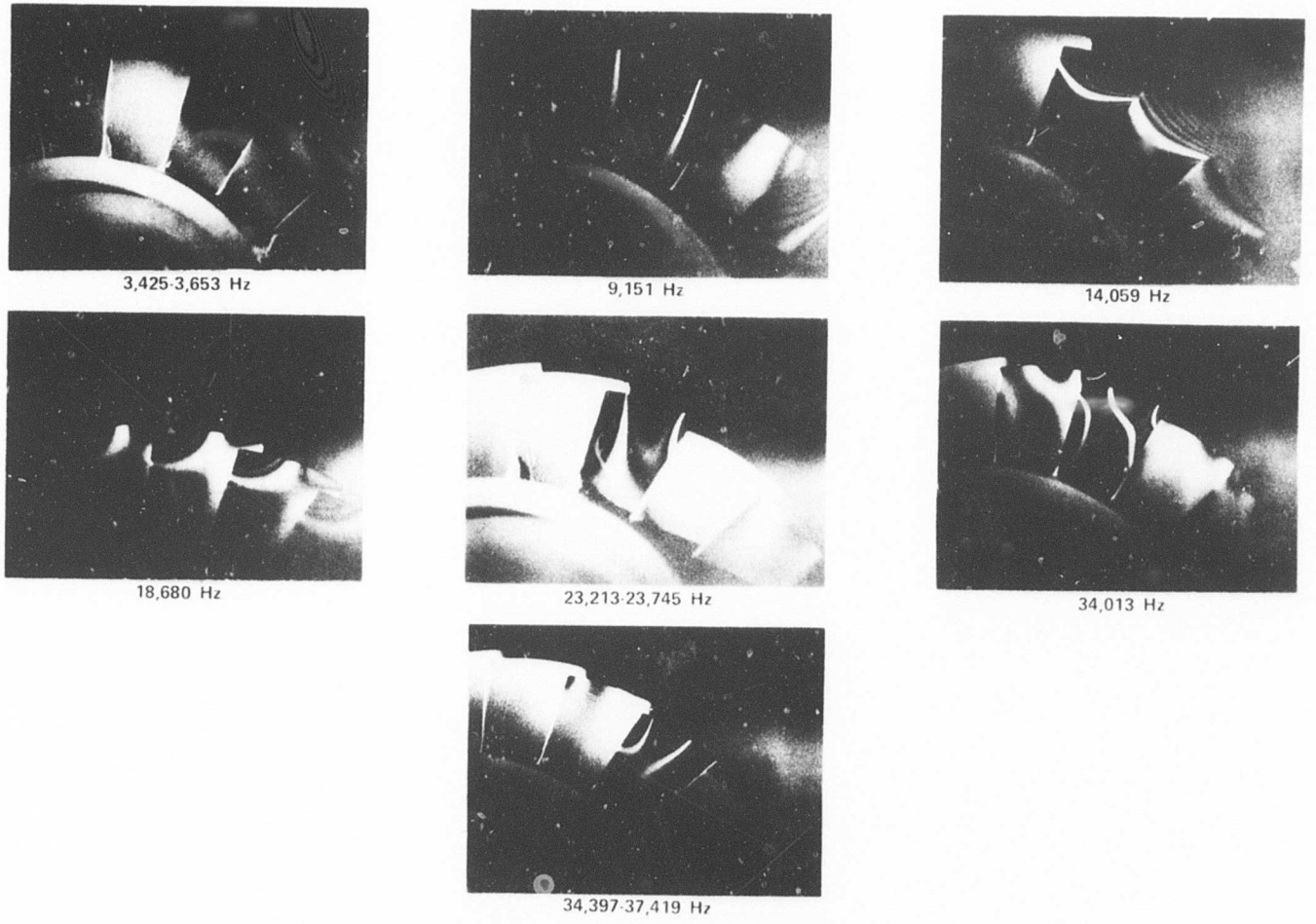

Figure 4. Reconstructed Time - Average Holograms Showing Nodal Patterns.

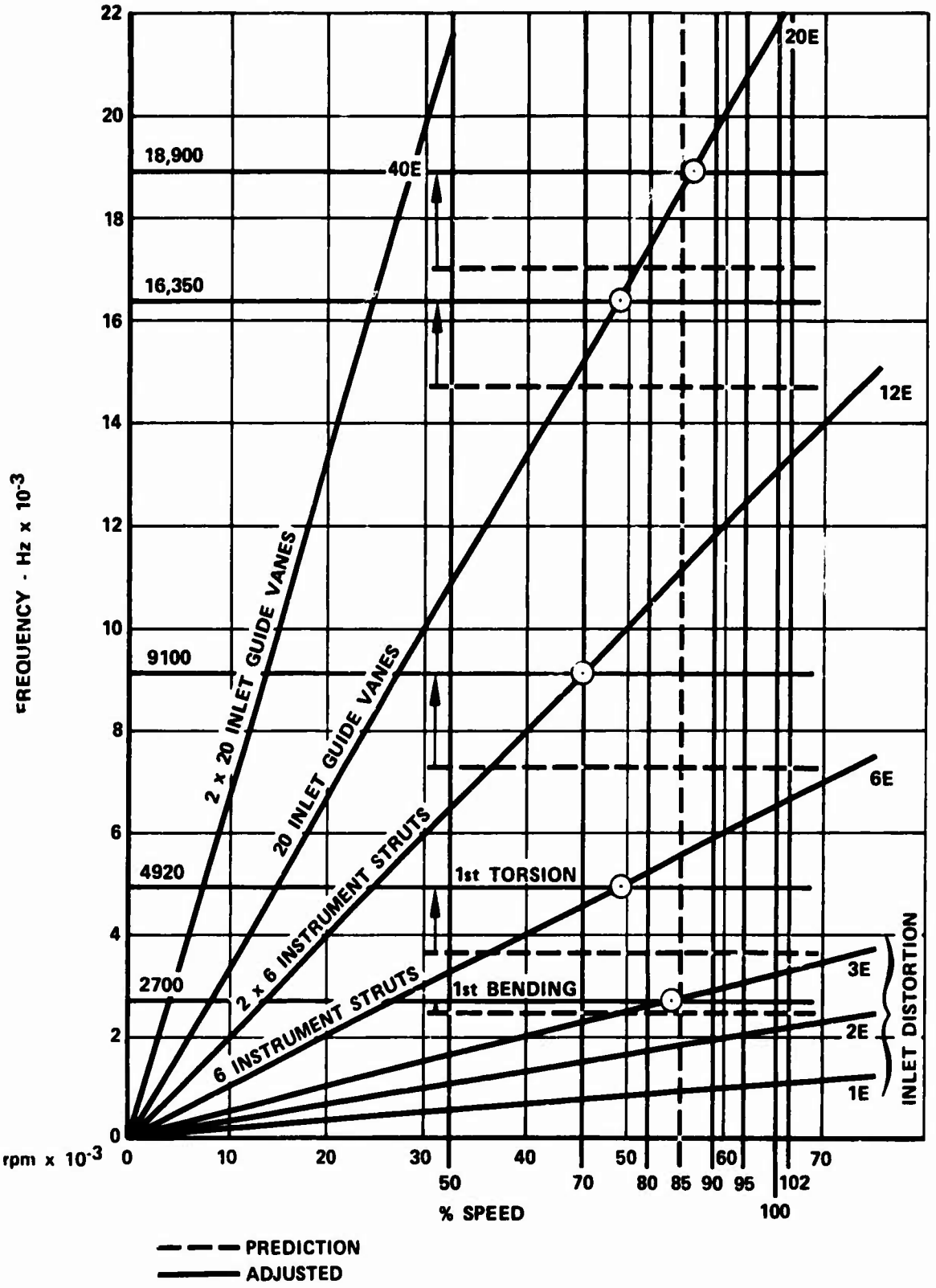

Figure 5. Modified Inducer Vibrational Characteristics.

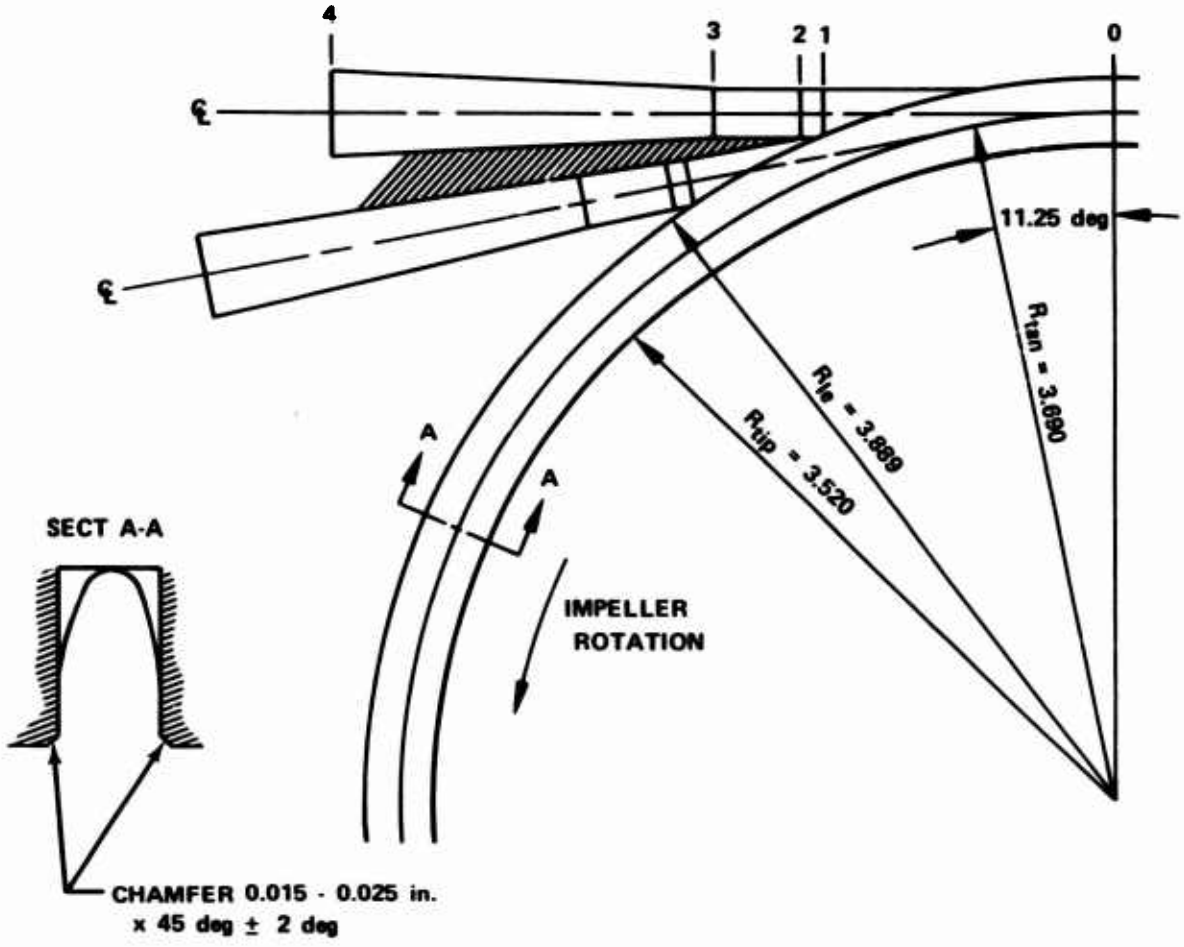

NUMBER OF PIPES	32
VANELESS SPACE HEIGHT	0.2300 in.
R_{le}/R_{tip}	1.105 in.
R_{tan}/R_{tip}	1.048 in.
BISECTOR ANGLE	17. 56 deg

CONE ANGLES		AREA RATIOS	
1-2	0 deg	1-2	1.0
2-3	3 deg	3-2	1.214
3-4	5 deg	4-2	3.433

PIPE DIAMETERS		DIFFUSER LENGTH	
1-	0.2300 in.	0-1	1.5311 in.
2-	0.2300 in.	1-2	0.1150 in.
3-	0.2534 in.	2-3	0.4463 in.
4-	0.4262 in.	3-4	1.9789 in.

Figure 6. Pipe Diffuser Design.

SECTION III

TEST EQUIPMENT

The compressor research rig incorporated both the compressor and drive turbine assembled as a single rotor, as shown in Figure 7. The radial inflow drive turbine had an integral, single-entry, double-exit configuration, thus forming a back-to-back, thrust-balanced arrangement. A schematic of the compressor rig is shown in Figure 8. It is the same aerodynamic configuration as that used in the 10:1 program except for the modified inducer, inducer shroud, and new diffuser. The rig was mounted in the high-speed compressor test stand, schematically illustrated in Figure 9. Sufficient horsepower is available for testing at sea level inlet conditions.

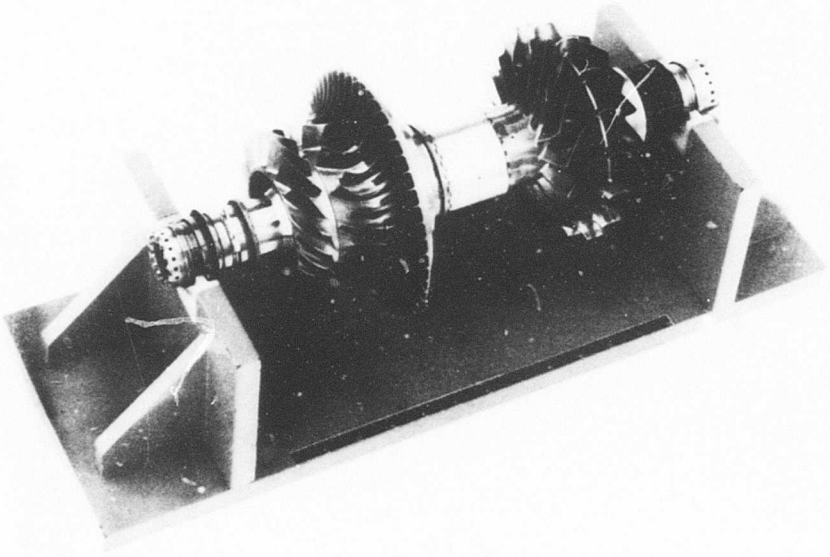

Figure 7. Rotor Assembly.

A bleed system was installed in the impeller exit shroud static pressure communicating groove, as shown in Figure 8. The bleed system could be controlled by the use of valves installed between the communicating groove and the scavenge pump. The thermal barrier machined between the impeller and inducer shroud, which was purged with nitrogen throughout the test to retard heat transfer, is also shown in Figure 8.

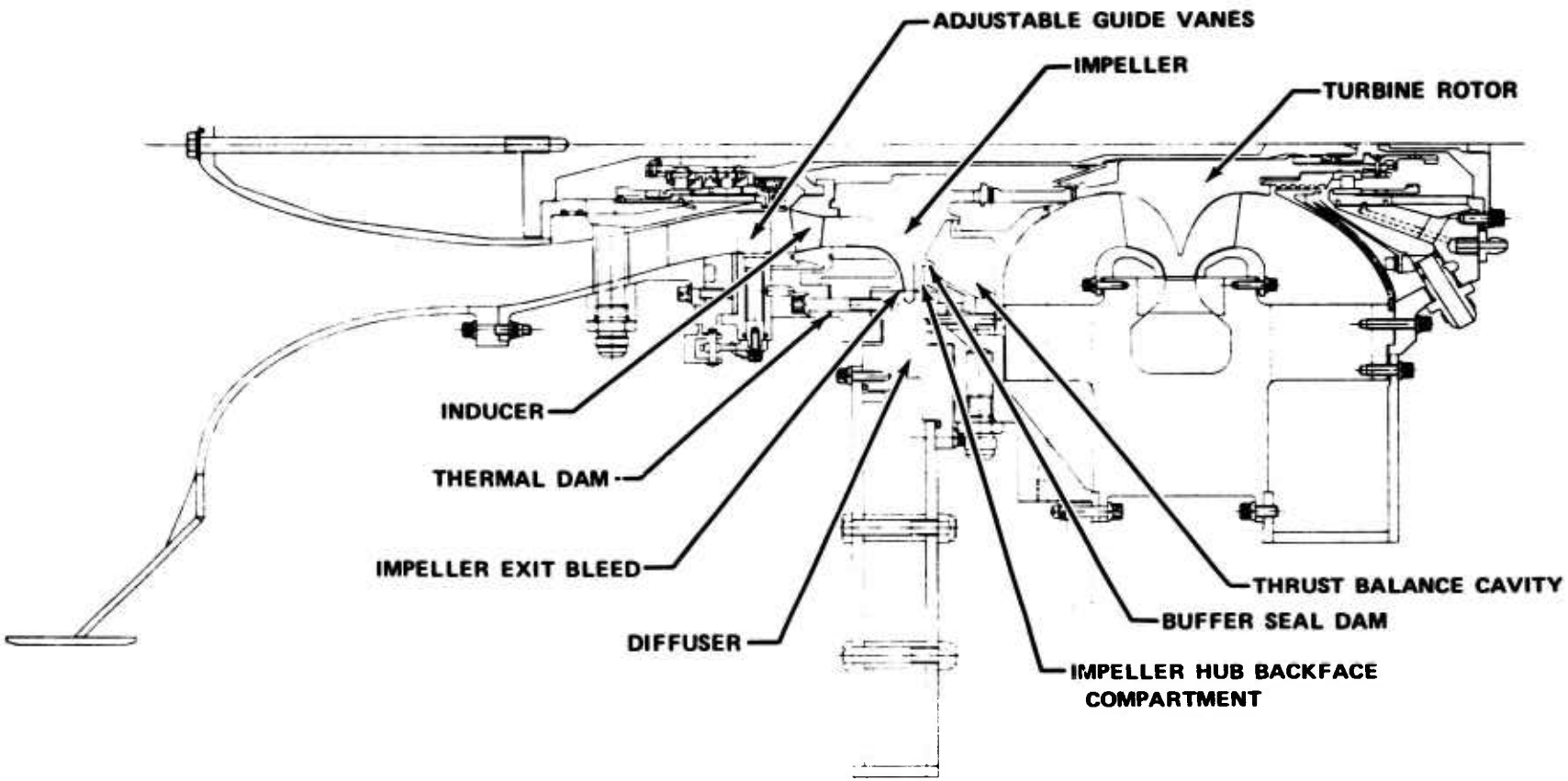

Figure 8. Modified Centrifugal Compressor Mounted on FRDC Drive Turbine.

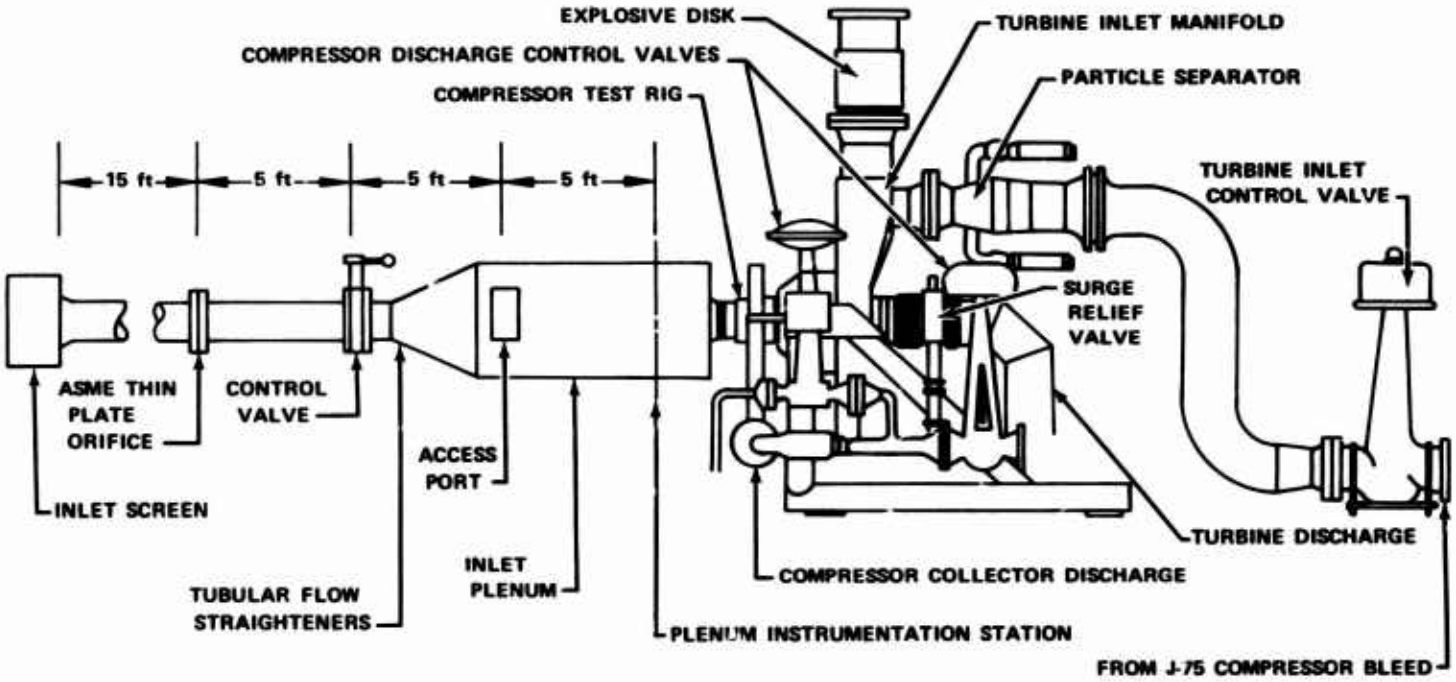

Figure 9. High-Speed Compressor Test Stand.

The impeller and inducer were detail-balanced by material removal. The final residual unbalance of the inducer after detail balance was 0.0016 oz-in. The impeller was detail-balanced to 0.0012 oz-in. in the front plane and 0.0020 oz-in. in the rear plane. The as-assembled and final residual rotor unbalances, which were obtained by insertion of pins and rivets, are as follows:

	Front Plane	Rear Plane
As Assembled	0.012 oz-in.	0.013 oz-in.
Final	0.001 oz-in.	0.0015 oz-in.

The final balance maximum unbalance limit in both the front and rear planes was 0.002 oz-in.

The inducer and impeller inlet radial and impeller tip axial rotor-to-shroud clearances were measured with removable rub probes after having reached 8%, 70%, 85% and 100% of design speed. Figure 10 contains the clearances measured in this test.

Rig vibrations were monitored on the test stand and recorded continuously on tape throughout the test. Figure 11 shows maximum 1E vibratory acceleration levels recorded for the front and rear bearings during a speed transient. The maximum front bearing acceleration was 54 g's and occurred at 63,000 rpm, which corresponds to a peak displacement of 0.00062 in. The rear bearing vibration remained relatively low, with the highest recorded vibration of 46 g's occurring at design speed. These vibrations are well below the maximum allowable limit of 270 g's. The bearing temperatures as a function of rotor speed are shown in Figure 12.

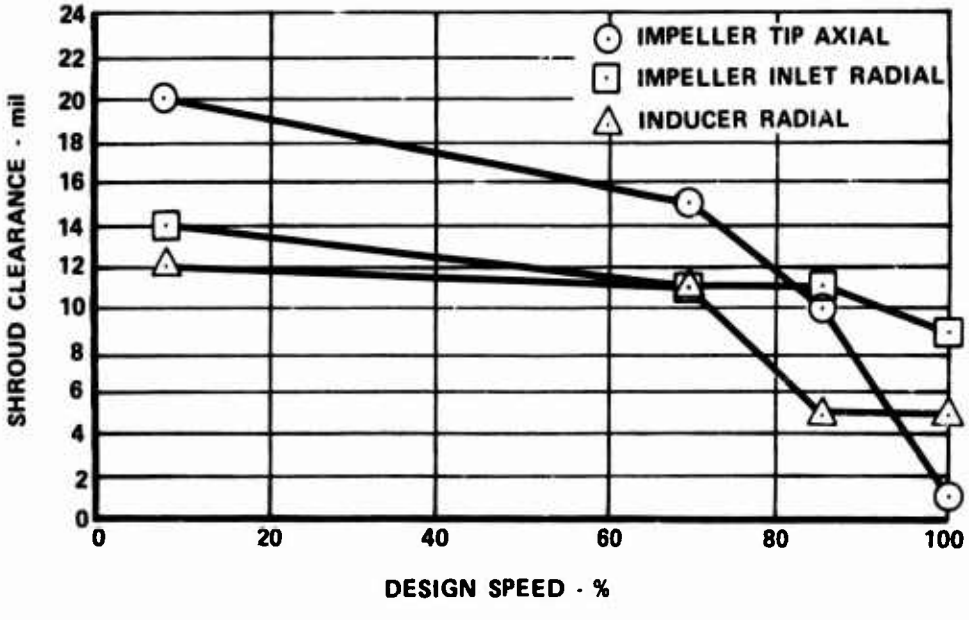

Figure 10. Shroud Clearance Measurements.

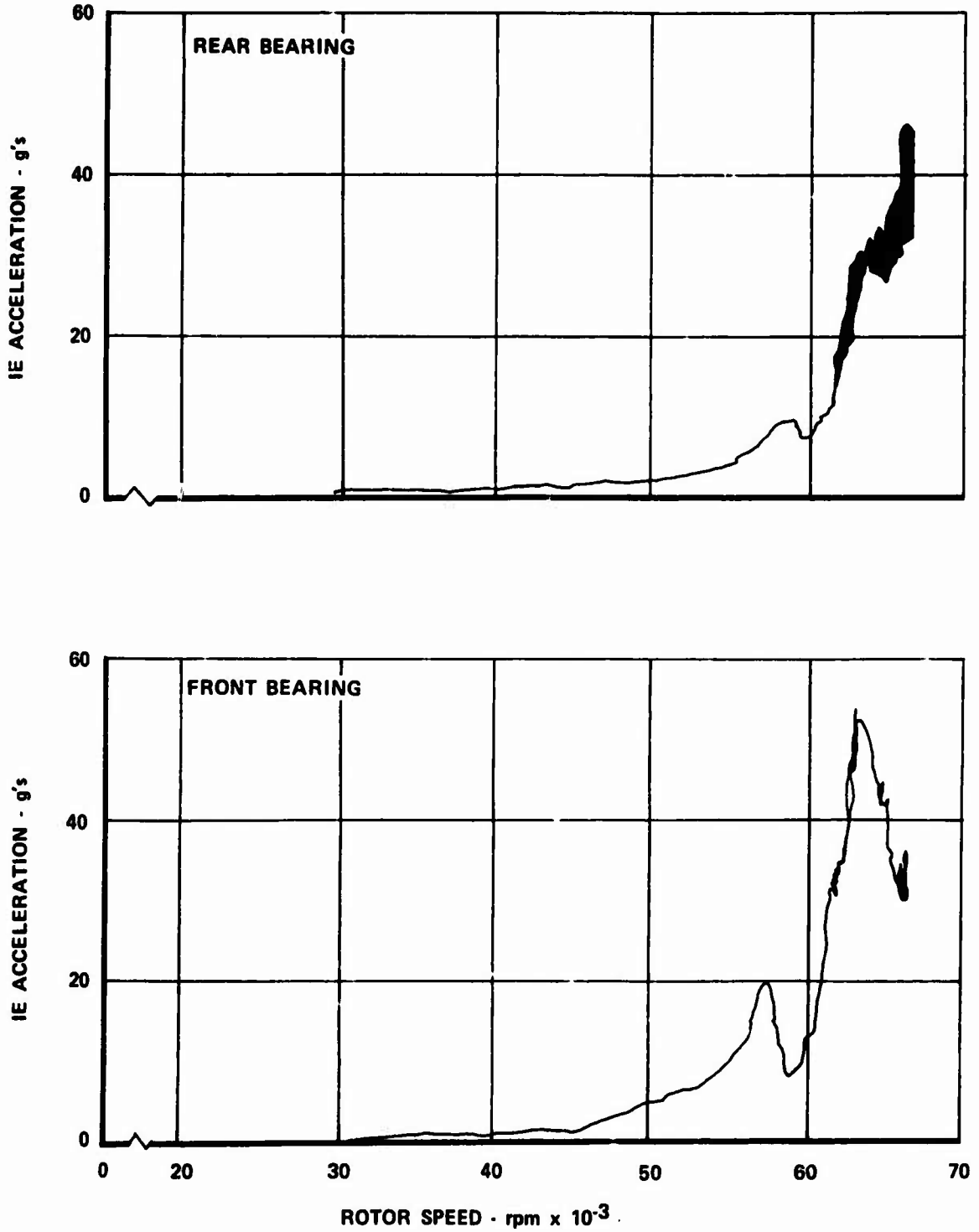

Figure 11. Maximum Bearing 1E Acceleration.

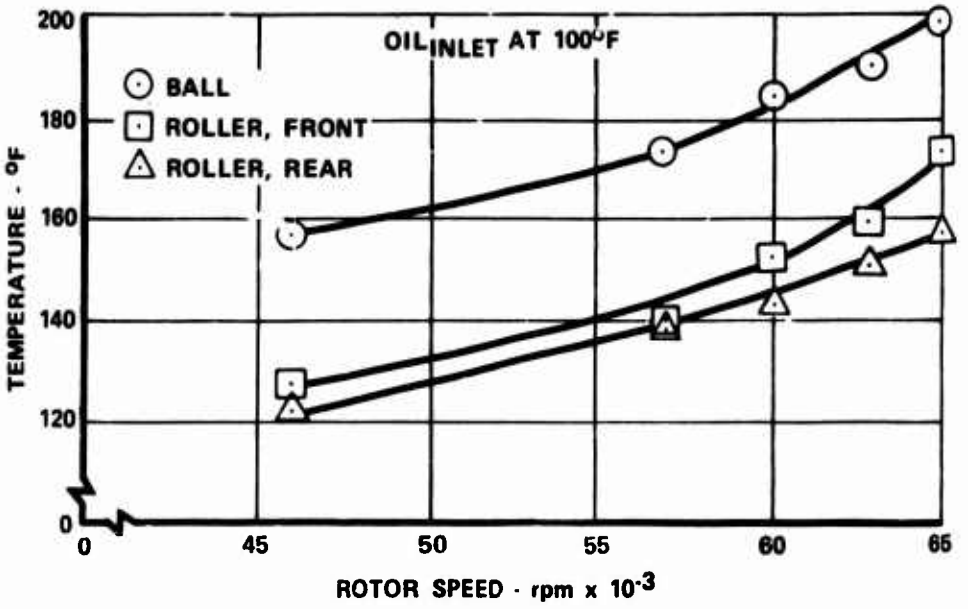

Figure 12. Bearing Outer Race Temperatures.

The impeller exit-to-diffuser entrance alignment is shown in Figure 13 and was calculated from build measurements obtained during compressor rig assembly and impeller-to-shroud clearances measured during the checkout test. The desired design speed alignment was such that the impeller blade exit and diffuser vaneless space centerlines were in line. At design speed, this alignment was essentially obtained within 0.0026 in. The small difference in alignment can be considered negligible since no forward-facing step was created, as the shroud sides of the impeller blades are in line with the diffuser vaneless space wall. An additional margin is allowed by the chamfer at vaneless space entrance.

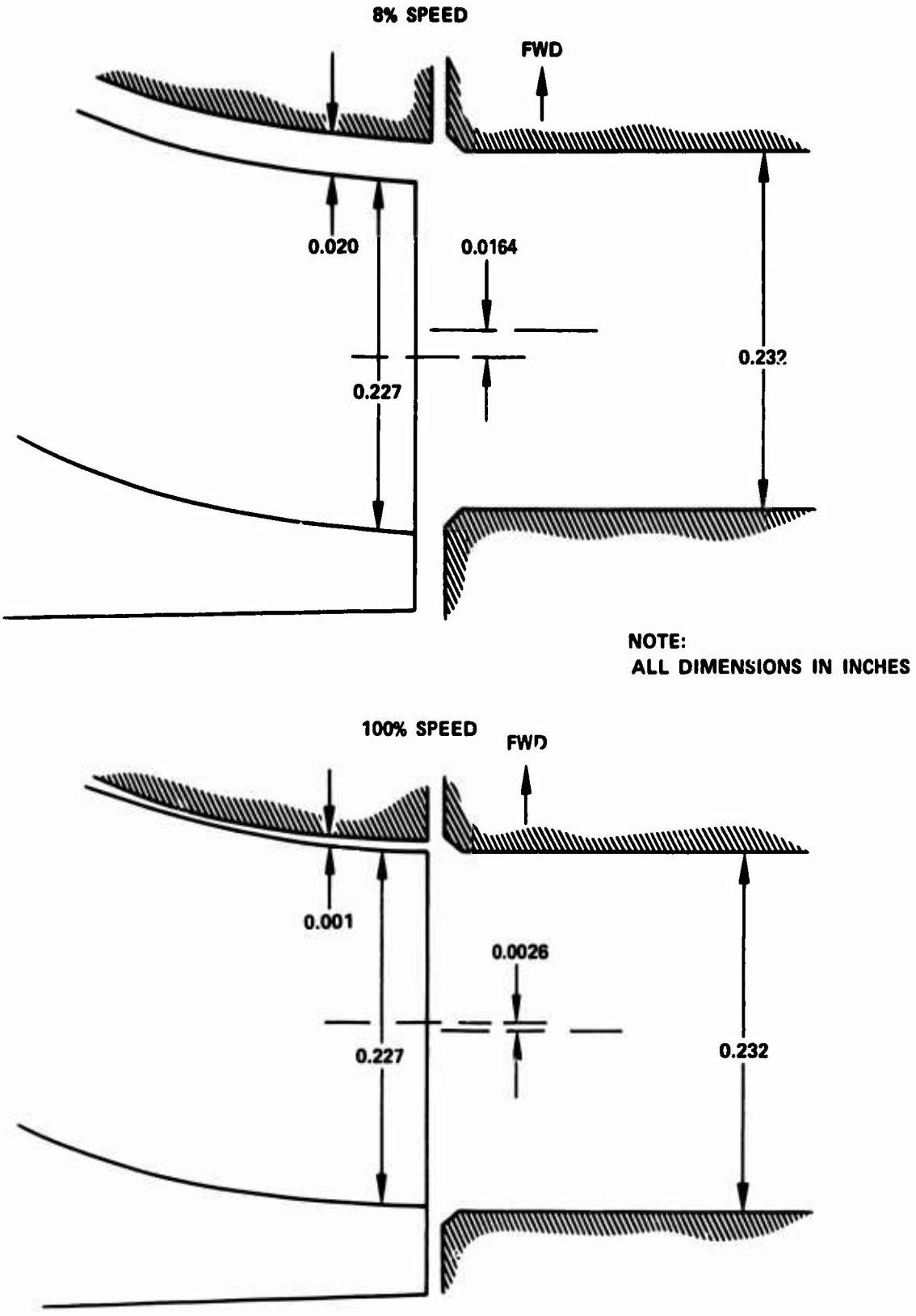

Figure 13. Impeller and Diffuser Alignment.

SECTION IV

INSTRUMENTATION

Instrumentation provided to permit evaluation of stage overall and inducer performance and to monitor rig operation is described below. Major instrumentation stations for the test compressor are defined in Figure 14, and an overall instrumentation schematic is shown in Figure 15.

OVERALL PERFORMANCE INSTRUMENTATION

Instrumentation was provided to obtain inlet flow rate, bleed flow rate, inlet guide vane position, impeller speed, and compressor inlet and discharge temperature and pressure. Overall performance instrumentation is described in detail below and is also summarized in Table 4.

Compressor inlet flow rate was calculated from data obtained from a 5.270-in.-diameter thin plate orifice installed upstream of the inlet plenum in a 12.5-in.-diameter inlet duct. The orifice was installed in accordance with ASME standards. Orifice upstream static pressure was measured by three static pressure taps, each sensed by a 0- to 15-psia transducer. Three orifice differential static pressures were each sensed by a 5-psid transducer. The temperature for the flow measurement was obtained by the inlet plenum instrumentation, which consisted of five Rosemount resistance thermometers installed at various radial positions in the inlet plenum to provide an area-averaged temperature.

Impeller rotational speed was obtained from two electromagnetic pickups mounted adjacent to a 6-tooth gear on the rear of the drive turbine rotor shaft. Inlet guide vane position was determined from measurements obtained from a potentiometer connected to the IGV actuator, which is calibrated based on physical actuator position vs vane stagger angle measurements obtained during assembly. Compressor inlet total pressure was measured with three Kiel-type total pressure probes located in the inlet plenum and connected to 0- to 15-psia pressure transducers.

A traverse probe was installed behind the inlet guide vanes to determine the radial total temperature distribution across the flow path at the rotor inlet station. The design of this probe is shown in Figure 16. The probe was aspirated and designed to eliminate conduction from the rig cases through the stem of the probe. The thermocouple leads were continuous to the uniform temperature reference to eliminate error from connectors and the lower quality wire that is generally used as extension wire. Data from this probe were used to determine the inlet temperature required in performance calculations, such as corrected weight flow, speed, and overall temperature ratio. The standard plenum instrumentation was used where inlet traverse temperature was not available.

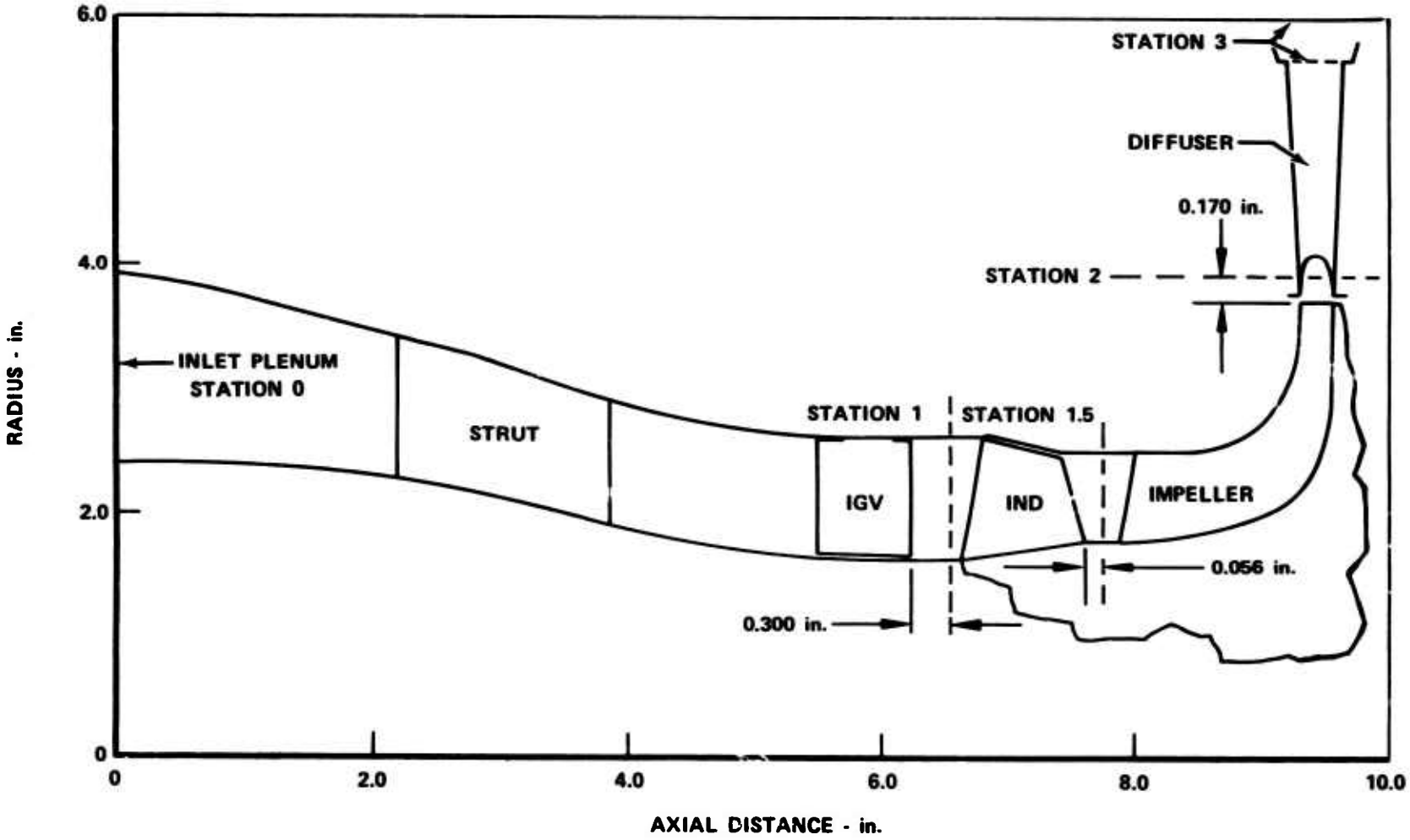

Figure 14. Compressor Flow Path and Instrumentation Station Locations.

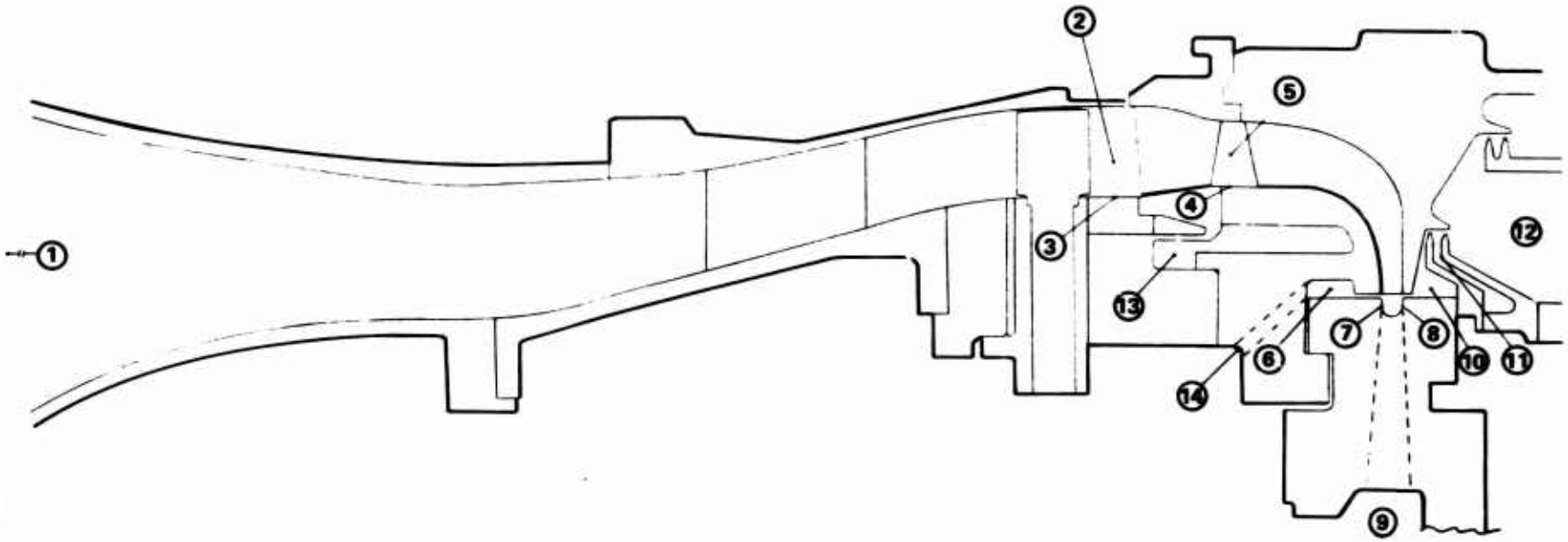

1. PLENUM - RESISTANCE TEMPERATURE BULBS (5)
   - TOTAL PRESSURE KIEL PROBES (3)
2. TOTAL TEMPERATURE TRAVERSE
3. STATIC PRESSURE TAPS (4)
4. STATIC PRESSURE TAPS (4)
5. AIR ANGLE, TOTAL PRESSURE AND TOTAL TEMPERATURE TRAVERSE
6. RIM STATIC PRESSURE TAPS (4) AND TOTAL TEMPERATURE
7. TANGENCY RADIUS SHROUD STATIC PRESSURE TAPS (4)
8. TANGENCY RADIUS HUB STATIC PRESSURE TAPS (4)
9. COLLECTOR - STATIC PRESSURE TAPS (7)
   - TOTAL TEMPERATURE PROBES (4)
10. BACKFACE STATIC PRESSURE (2) AND TOTAL TEMPERATURE
11. BUFFER SEAL STATIC PRESSURE (2)
12. THRUST BALANCE STATIC PRESSURE (2)
13. SHROUD CAVITY AIR TEMPERATURE
14. BLEED ORIFICE STATIC PRESSURE, DIFFERENTIAL PRESSURE, AND TOTAL TEMPERATURE

Figure 15. Modified Centrifugal Compressor Test Instrumentation.

TABLE 4. COMPRESSOR OVERALL PERFORMANCE INSTRUMENTATION SUMMARY

Location	Flow Variable	Instrument Type	Quantity
Inlet Duct	P_s	Orifice Wall Tap	3
	ΔP_s	Orifice Wall Tap	3
Plenum	P_t	Kiel Head	3
	T	Rosemount	5
Inlet Guide Vane	α	Potentiometer	1
IGV Exit	T	Aspirated Traverse Thermocouple	1
Bleed Orifice	P_s	Wall Tap	1
	ΔP_s	Upstream-Downstream	1
	T	C/A Thermocouple	1
Collector	P_s	Wall Tap	7
	T	Aspirated Thermocouple	4
Rotor Speed	Speed	Electromagnetic Pickup	2

Compressor exit static pressure was measured by seven static pressure taps in the collector: six connected to a pressure-scanning system using a 0- to 150-psia transducer, and one connected to a 0-200 psia close-coupled transducer for fast response during surges. The taps were located on the shroud-side wall so that neither diffuser discharge velocity nor the collector struts interfere with the measurements. The design and location of these taps are shown in Figure 17. Compressor exit total temperature was measured with four chromel-alumel (C/A) thermocouples in the discharge collector aligned on diffuser pipe centerlines. A tabulation of the pressure tap and thermocouple locations is given in Table 5. To increase the accuracy of the temperature measurements, the thermocouples were constructed such that the sensor was located in a flow stream that was aspirated to ambient. Placement of the sensor in the high-velocity flow reduced measurement errors caused by thermal conduction. In addition, the thermocouples were constructed from a single batch of calibrated, special-limits-of-error wire similar to the IGV exit probe. This wire was also continuous from the thermocouple junction to the reference junction.

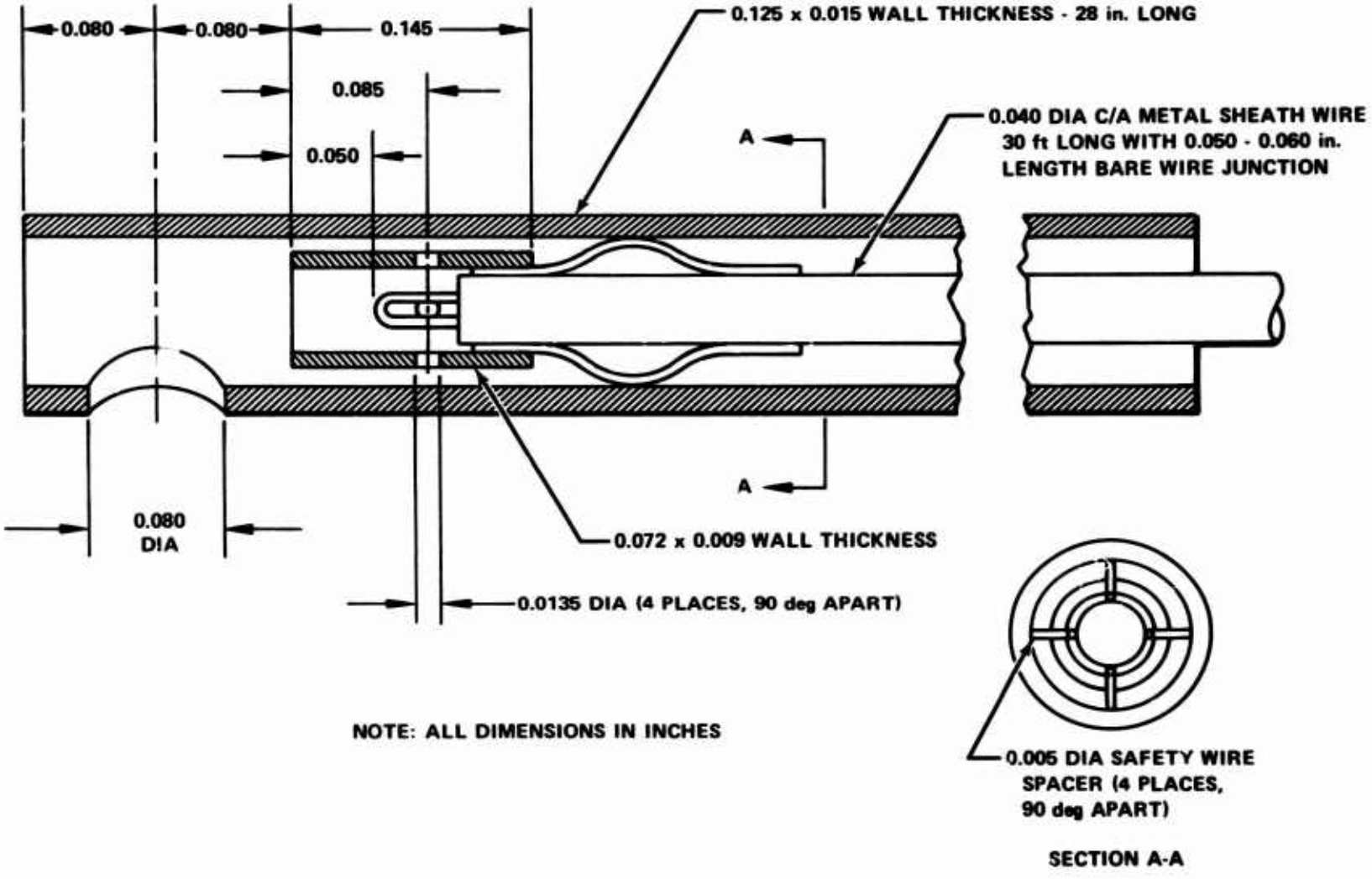

Figure 16. IGV Exit Temperature Traverse Probe.

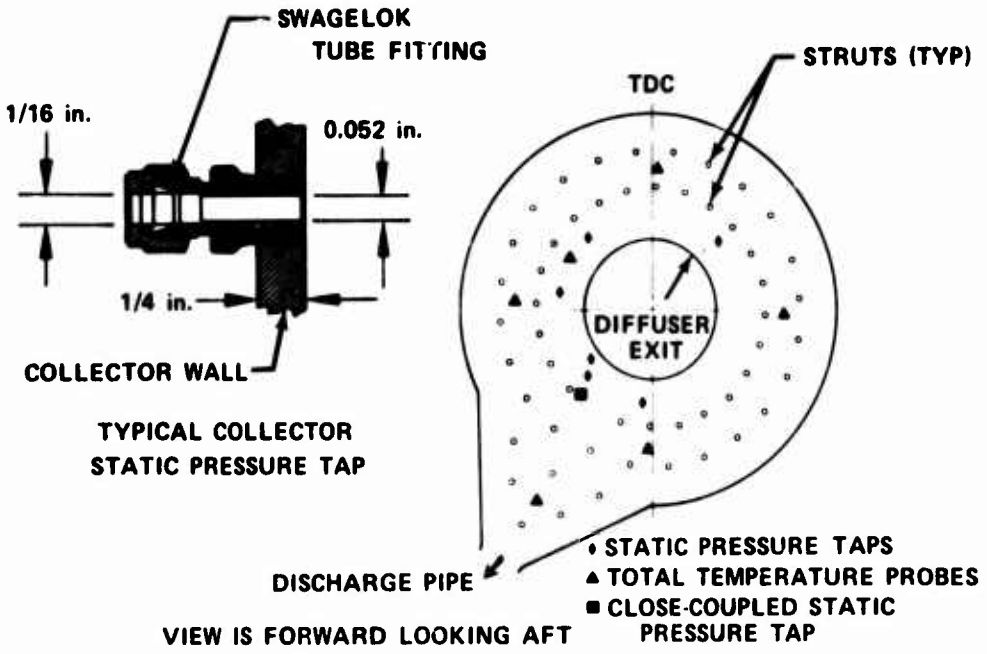

Figure 17. Collector Instrumentation Locations.

COMPONENT PERFORMANCE INSTRUMENTATION

Instrumentation was provided to evaluate the performance of the modified inducer. The component performance instrumentation is described below and summarized in Table 6. Static pressure at station 1 was measured by four equally spaced shroud wall taps. Radial distributions of total pressure, total temperature, and air angle at the inducer exit (station 1.5) were obtained by a radially traversing cobra probe and thermocouple. The cobra probe and thermocouple are shown in Figure 18. The pressure ports were constructed from 0.020-in.-OD tubing. Additionally, four static pressure taps were equally spaced about the circumference on the shroud wall in the plane of the traversing cobra probe.

Instrumentation was provided to measure impeller tip static pressure on both the shroud side and the hub side. Impeller tip static pressure on the shroud side was obtained from measurements of the pressure in a circumferential passage that was connected with the flow path by a 0.022-in.-wide circumferential groove between the shroud housing and the diffuser. Pressure was measured through four ports that were equally spaced around the circumference. This circumferential groove scheme is shown in Figure 19. Impeller tip backface pressure was measured by two 0.062-in.-diameter tubes installed 180 deg apart in the impeller tip backface cavity.

Instrumentation was provided to measure wall static pressure on both the hub and the shroud side in the diffuser vaneless space at station 2. These static pressure taps are 0.020 in. in diameter and were made by an electrical discharge machining process to eliminate drilling burrs and to ensure sharp edges at the intersection of the pressure port and the diffuser passage. These taps were located on diffuser pipe centerlines at the diffuser tangency radius.

TABLE 5. LOCATION OF COLLECTOR INSTRUMENTATION

Probe	Axial Location**	Radial Location, in.	Circumferential Location, deg***
Static Tap			
1	S	7.5	46
2	S	7.5	316
3	S	7.5	281
4	S	6.4	231
5	S	7.5	226
6*	S	9	221
7	S	7.5	181
Thermocouple			
1	M	11.0	3
2	M	11.0	93
3	M	11.0	183
4	M	11.0	273

*Connected to close-coupled transducer

**S–Shroud side
M–Midway between collector manifold walls

***Circumferential location is measured clockwise from TDC, forward looking aft.

TABLE 6. COMPRESSOR COMPONENT PERFORMANCE INSTRUMENTATION SUMMARY

Location	Flow Variable	Instrument Type	Quantity
Station 1	T	Radial Traversing Thermocouple	1
	P_S	Shroud Wall Tap	4
Station 1.5	P_S	Shroud Wall Tap	4
	P_t, T, α	Radial Traversing Cobra Probe With Thermocouple	1
Impeller Tip, Shroud Side	P_S	Communicating Groove	4
Impeller Tip, Backface	P_S	Tube	2
Station 2	P_S	Shroud Wall Tap	4
	P_S	Hub Wall Tap	4

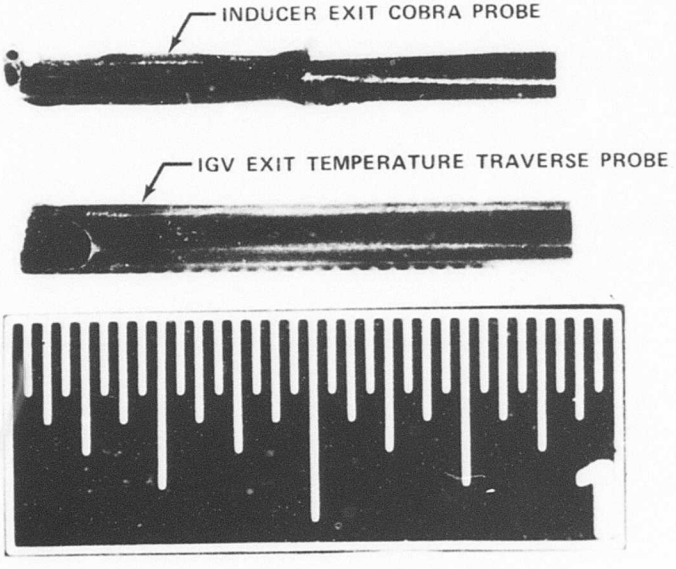

Figure 18. Traverse Probes.

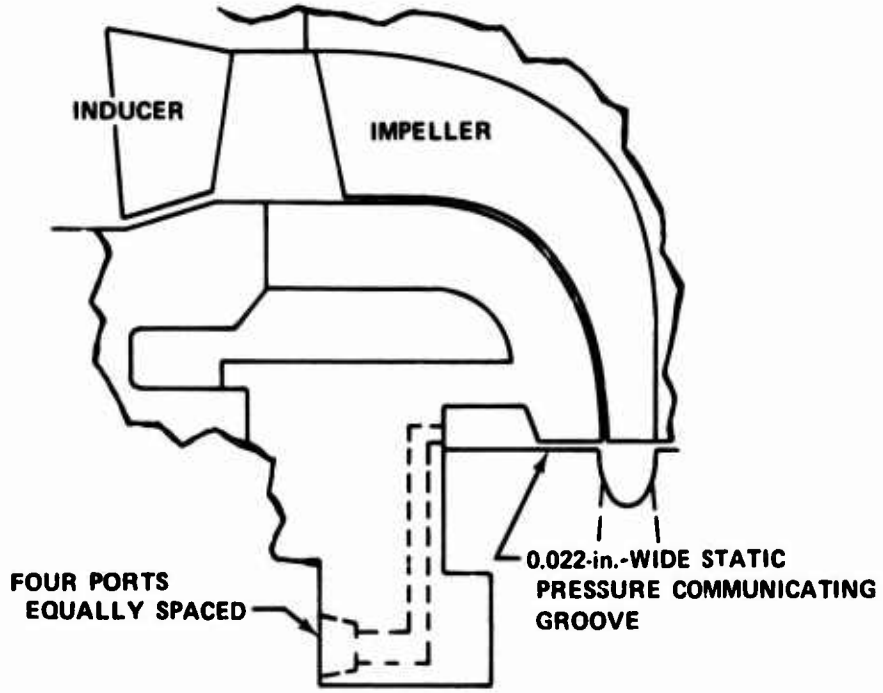

Figure 19. Impeller Tip Static Pressure Passage.

SPECIAL INSTRUMENTATION

Total pressure in the plenum and static pressure in the collector manifold were measured with close-coupled transducers to achieve the fast response required to define overall performance as the compressor surged.

DATA READOUT AND RECORDING SYSTEM

All compressor rig data were recorded with an automatic digital magnetic tape recorder. Information needed for safe operation of the rig and for setting data points was displayed in the control room. Control room data readouts included rotor speed, rig vibration levels, bearing temperatures, oil pressure, inlet orifice differential pressure, impeller thrust balance pressure, rig inlet pressure, and rig discharge pressure. When cobra probe data were being obtained, the total pressure measured by the cobra probe was displayed on an X-Y plotter located adjacent to the traverse actuator controls. This allowed changing the speed or stopping the cobra probe actuator to allow the probe to respond to changes in the airflow angle.

SECTION V

PROCEDURES

TEST PROCEDURES

A checkout test was conducted to: (1) verify satisfactory compressor rig mechanical operation, (2) check the instrumentation and the data acquisition system, and (3) provide preliminary overall performance information.

The compressor rig operated satisfactorily over its entire range of operation. During the checkout test, bearing vibrations and temperatures, bearing oil flow pressure, rotor thrust balance pressure, and rotor clearances were monitored, and no problems were observed. The instrumentation and data acquisition system operated properly during the checkout test. Minor instrumentation changes were made prior to performance data acquisition.

Preliminary overall performance was obtained at 70% speed, 85% speed, and a matrix of speed and IGV settings from 90% to 100% speed and -5 deg to 10 deg IGV settings. This matrix of data enabled the choosing of speeds and IGV settings required to obtain optimum 10:1 and 8:1 pressure ratio speed lines. A summary of the data points acquired in the checkout and performance tests is given in Table 7.

Performance tests were conducted to obtain overall compressor and component inducer performance. Overall compressor performance was defined by speed-line stall transients and by steady-state points at near-stall, wide-open discharge, and several intermediate points. Slow-stall transients were first performed by recording data at a rate of 1 scan/sec while closing the compressor discharge valve from its wide-open position (thus increasing backpressure) until the rig surged. During the transient, adjustments to the turbine inlet control valves were made to hold the rotor rpm constant. A near-stall point was then set, based on the collector static pressure, and the compressor was again operated into stall while recording data at 10 scans/sec. Steady-state data points were distributed along a speed line based on the collector static pressure range recorded during the first slow-stall transient. A steady-state point consisted of cycling the pressure scanning units twice at a rate of 2 ports/sec, followed by the recording of the rest of the rig instrumentation for 10 sec at a rate of 10 scans/sec. Inlet guide vane temperature traverse data were obtained at near-stall points for four different speeds.

Inducer component performance data were obtained by radially traversing an air angle, total pressure, and total temperature probe behind the inducer. These traverses were performed by running the probe into its limit and then recording data while slowly retracting the probe out of the flow path. The data recording rate for all traverses was 1 scan/sec. Total pressure vs radial travel data were monitored in the control room on an X-Y plotter, and the traverse rate was governed, as required, to obtain good profile definition.

TABLE 7. DATA SUMMARY

Approximate Speed	IGV, Setting (deg)	Steady State		Stall Transients		IGV Exit Traverse		Inducer Exit Traverse	
		Checkout	Performance	Checkout	Performance	Checkout	Performance	Checkout	Performance
30%	30				1				
	40				1				
70%	20	1	4	1	2		1		
	30		3		1				
85%	20	1	4	1	1		1		1
	30		3		1				
90%	-5			1					
	0			1					
	10			1					
94%	-5			2					
	0			1					
	10			1					
	15		6		1		1		1
	20		6		1		1		1
98%	-5			1					
	0			1					
	10			1					
100%	-5	3		1					
	0	5		3		1		1	
	0		6		2		1		1
	0*		3		3				
	5		5		1		1		1
	10	3		1					

*Impeller Exit Boundary Layer Bleed

DATA REDUCTION PROCEDURES

Overall Performance

The reduction of overall performance data was accomplished through the use of an IBM 370 computer program. All performance data, except orifice and plenum data, were corrected to standard day inlet conditions based on the plenum pressure and mass-average total temperature at the inlet guide vane exit as follows:

$$\text{corrected pressure} = \frac{\text{recorded pressure}}{\delta}$$

$$\delta = P_{t_0}/14.696$$

$$\text{corrected temperature} = \frac{\text{recorded temperature}}{\theta}$$

$$\theta = \overline{T}_1/518.688$$

The actual inlet orifice weight flow was calculated from the orifice equation:

$$W_{act} = K_1 \left[C - K_2 \left(\frac{\Delta P_s}{P_s} \right) \right] \left[\frac{P_s \cdot \Delta P_s}{T} \right]^{1/2}$$

where

P_s = upstream orifice static pressure (psia)

ΔP_s = orifice differential static pressure (psia)

T = orifice flow total temperature (°R)

$C = 1.0$

$K_1 = 14.675$

$K_2 = 0.302$

Actual bleed orifice flow was calculated from

$$\left(W_{act}\right)_{bl} = \frac{k \cdot P_s}{\sqrt{T}}$$

where

$k = f(\Delta P_s/P_s)$

Both weight flows and rotor speed were corrected to standard day inlet conditions as follows:

$$W = W_{act} \frac{\sqrt{\theta}}{\delta}$$

$$N_{cor} = \frac{N_{act}}{\sqrt{\theta}}$$

Overall temperature ratio and total-to-static pressure ratio are given, respectively, by

$$TR = T_3/518.688$$

$$PR = P_{s3}/14.696$$

At steady-state points, the overall pressure ratio was based on the arithmetic average of six collector static pressure taps read through a pressure scanning system. During stall transients, the pressure ratio was determined from a single collector static pressure tap read through a close-coupled pressure transducer.

The overall adiabatic efficiency was defined as

$$\eta = \frac{\text{ideal (isentropic) enthalpy change}}{\text{actual enthalpy change}} = \frac{\Delta hf\ (PR)}{\Delta hf\ (TR)}$$

where Δh (PR) and Δh (TR) were determined by fourth-degree curve fits of change in enthalpy vs pressure ratio and temperature ratio data from table 1 (Dry Air Tables) in Keenan and Kaye Gas Tables.[c] This method automatically compensates for the variation in specific heat as a function of temperature.

For data obtained while the impeller exit bleed system was activated, a net weight flow and a net adiabatic efficiency, which accounts for the work done on the bleed flow, were defined as follows:

$$W_{net} = W_0 - W_{bl}$$

$$\eta_{net} = \frac{W_{net} \cdot \Delta hf\ (PR)}{W_{net} \cdot \Delta hf\ (TR) + W_{bl} \cdot \Delta hf\ (TR_{bl})}$$

where

$$TR_{bl} = T_{bl}/518.688$$

T_{bl} = temperature of the bleed flow (°R)

---

[c]Keenan and Kaye, Gas Tables, John Wiley & Sons, Inc., New York, September 1963.

Overall performance data used for direct comparison with data from the 10:1 program were reduced by the same methods as above, except that the temperatures were corrected to the plenum temperature rather than the inlet guide vane exit mass-average temperature. This was done to maintain a common method of data reduction and to provide a valid comparison of the two sets of data since no performance corrections for inlet heating effects were applied to 10:1 program data.

Inlet Guide Vane Performance

Inlet guide vane performance, in terms of total pressure loss and turning distribution vs inlet weight flow and guide vane setting, was assumed to be equal to the inlet guide vane performance demonstrated under the 10:1 program since the same vanes and inlet system were used. However, the radial total temperature distribution at the inlet guide vane exit, which was assumed to be a constant 518.688°R for the 10:1 program, was measured and mass-averaged across the span as follows:

$$\bar{T}_1 = \sum_{i=1}^{n} \Delta W_i \cdot T_i / \sum_{i=1}^{n} \Delta W_i$$

where

$$\Delta W_i = \frac{k \cdot \Delta A_i \cdot P_{ti}}{\sqrt{T_i}} \sin \alpha_i$$

IGV exit total temperature traverses at 15 and 20 deg IGV turning and 94% design speed were recorded with the temperature probe in an IGV wake. This was not consistent with the remainder of the traverses recorded on other speed lines, which were taken out of an IGV wake. Therefore, the IGV exit mass-average temperature for these two speed lines was determined from the measured collector total temperature and a plot of compressor temperature ratio vs rotor speed squared as a function of IGV setting.

Inducer Performance

Inducer performance and velocity triangles were calculated through the use of an IBM 370 streamline analysis computer program, P&WA Deck 8204. This program, shown schematically in Figure 20, satisfies the continuity, energy, and radial equilibrium equations from input descriptions of the compressor geometry, airflow, rotor speed, total pressure and air angle profiles at the IGV and inducer exits, total temperature profile at the IGV exit, and design blockage distributions. Because of wall and probe hole effects on the traverse probe measurements in the regions within approximately 0.030 in. of the flow-path walls, free-stream air angle and total pressure traverse data were faired by hand to the walls in this area. Adjustments were then made to the blockage distributions until the calculated shroud static pressures at the IGV exit and inducer exit instrumentation stations matched those measured. This is an accepted method of data reduction for axial flow compressors and was considered to provide increased accuracy over the IBM 1130 digital computer program, CCDRP (Centrifugal Compressor Data Reduction Program), used during the 10:1 program to calculate inducer performance.

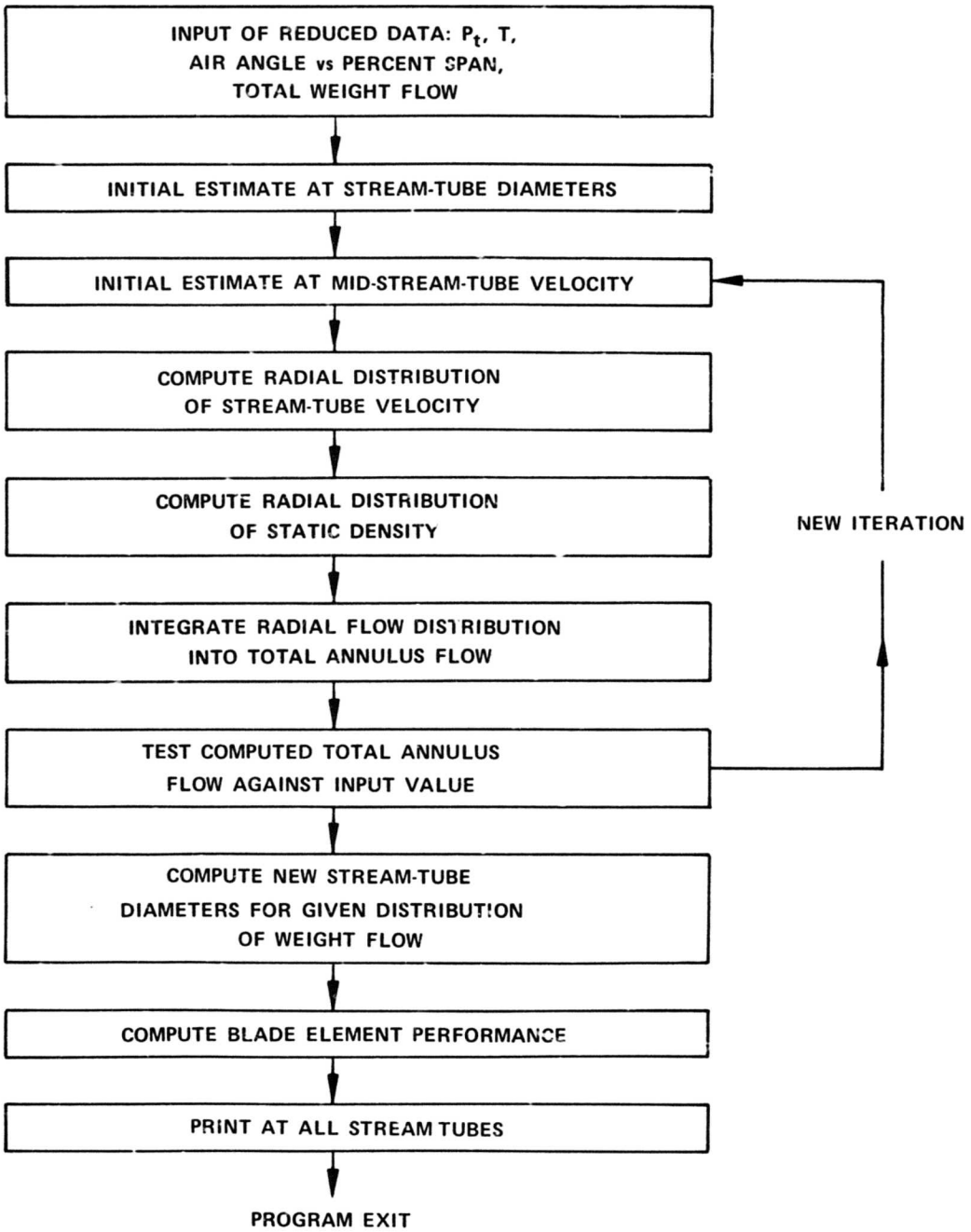

Figure 20. Schematic of 8204 Streamline Analysis Program Flow Path.

Again, as was done for overall performance data, inducer performance data to be used for comparison with data obtained during the 10:1 program were reduced by the same methods to provide a valid comparison. Total pressure, total temperature, air angle, and radial travel data from each inducer traverse were input into the CCDRP IBM 1130 program. A linear approximation of the static pressure distribution calculated by the streamline analyses program was used.

The ratio of specific heats (γ) was determined from a curve fit of γ vs static temperature (T_S) data and involved an iteration on the value of T_S to satisfy the following at each percentage of span:

$$P_t/P_s = \left(\frac{T}{T_s}\right)^{\frac{\gamma}{\gamma-1}}$$

The absolute Mach number (M) was calculated from the relationship

$$M = \left\{\left[(P_t/P_S)^{\frac{\gamma-1}{\gamma}} - 1\right]\frac{2}{\gamma-1}\right\}^{1/2}$$

The local speed of sound was calculated by

$$a = \left(\gamma GRT_s\right)^{1/2}$$

Total temperature measurements were corrected for Mach number effects by dividing the recorded temperatures by a probe recovery factor. The recovery factor used in the calculations was based on the actual probe recovery factor vs Mach number calibration data. Total pressure and total temperature were then mass-averaged across the span.

The sum of the incremental weight flows from the mass-averaging routine was checked against the corresponding inlet orifice flow, and an iteration was performed on the air angle values until the two flow calculations agreed. Final mass-average total pressure ($\overline{P}_{t1.5}$) and total temperature ($\overline{T}_{1.5}$) values were then calculated, based on the adjusted air angle profile. Inducer pressure ratio and temperature ratio were calculated as follows:

$$PR_{(1-1.5)} = \overline{P}_{t1.5}/\overline{P}_{t1}$$

$$TR_{(1-1.5)} = \overline{T}_{1.5}/518.688$$

Inducer efficiency was calculated by the same methods as the overall efficiency and is given by

$$\eta_{ind} = \frac{\Delta hf(PR_{1-1.5})}{\Delta hf\,(TR_{1-1.5})}$$

From M, a, and α, the components of the velocity triangles, as defined below, at each percentage of span were then calculated.

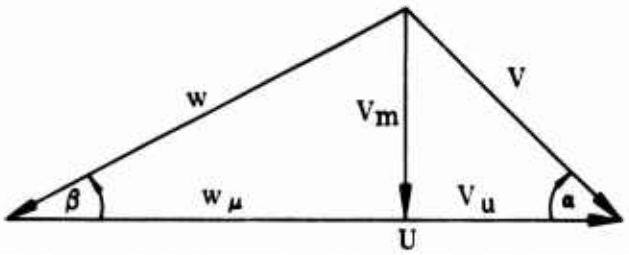

Impeller incidence (i) was determined at each percentage of span by

$$i = \beta^* - \beta$$

where β^* is the impeller leading-edge metal angle at the corresponding percentage of span.

Rotor Performance

Combined inducer-impeller performance was determined through the use of an internal flow analysis computer program, which involves the solution of the equations of continuity and momentum. Input for the analysis consisted of overall static pressure ratio and total temperature ratio, rotor speed, mass flow, impeller exit static pressure, configuration geometry, flow factors at the leading edge of the inlet guide vanes and impeller exit, and a calculated temperature rise due to shroud friction, based on rotor speed, density, surface area, and friction coefficient for bladed disks.

SECTION VI

VALIDATION OF TEST DATA

Estimates of the uncertainty of the data acquired from the test rig are presented in Table 8. These estimates include the uncertainty of both the sensor and the recording device. Uncertainty of air angle assumes no alignment error. Both bias (constant error) and precision errors (precision errors are two standard deviations from the mean) were used to determine the potential uncertainty, and are presented in Table 8. When multiple probes were available for redundant measurement, the precision error was calculated by statistically averaging individual measurements, as illustrated below.

$$u = \frac{e}{\sqrt{n}}$$

where

u = overall uncertainty of flow variable

e = uncertainty of individual sensor

n = number of sensors recording the same flow variable

Table 8 also includes the effect of the data uncertainty on the uncertainty of the overall efficiency performance calculation. This performance uncertainty estimate was calculated by the method of partial derivatives for error analysis of a complex function. The uncertainty of the efficiency value at the design point was 0.54 percentage point.

An estimate of the uncertainty of the inlet orifice flow measurement is shown in Figure 21 as a function of inlet orifice flow rate and was ±1.84% at design flow. The uncertainty of the impeller exit bleed flow measurement is estimated to be approximately 4.0% of the measured flow rate.

At each steady-state point, approximately 20 scans of data recorded over a 2-sec interval were averaged. A typical printout from a near-stall, steady-state point at 99% design speed and 0-deg inlet guide vane setting is shown in Table 9. A 2-sec average value, the maximum and the minimum values recorded, and a 3-sigma value (three standard deviations from the mean) are also listed for each instrumentation. These provide a measure of the actual scatter in the data due both to the uncertainty in measurement and to slight speed and flow variations that may have occurred while recording the steady state.

TABLE 8. ANALYSIS OF INSTRUMENTATION ACCURACY

Variable	Location (Station)	Type Instrument	Range	Number of Probes Averaged	Bias, ±	Precision, ±	Uncertainty, ±	Units
P_s	0	Transducer	0 to 15	3	0.04	0.01	0.05	psia
T	0	Resistance Thermometer	Ambient	5	0.27	0.07	0.34	°R
T	1	CA/TC	0 to 650	1	0.39	0.64	1.03	°R
P_s	1 and 1.5	Pressure Scanner	0 to 15	4	0.05	0.02	0.07	psia
Air Angle	1.5	Potentiometer	0 to 160	1	0.4	1.2	1.6	deg
P_t	1.5	Transducer	0 to 25	1	0.07	0.04	0.11	psia
T	1.5	CA/TC	0 to 600	1	3.0	1.2	4.2	°R
P_s	2 and 3	Pressure Scanner	0 to 150	1	.43	0.34	0.77	psia
T	3	CA/TC	0 to 1150	4	0.90	0.48	1.38	°R
Flow Rate	Inlet	Orifice	3.1	3 ΔP, 3 P_s, 5 T	0.024	0.037	0.059	lb/sec
Efficiency	0 to 3	-	75%	-	-	-	0.538	%

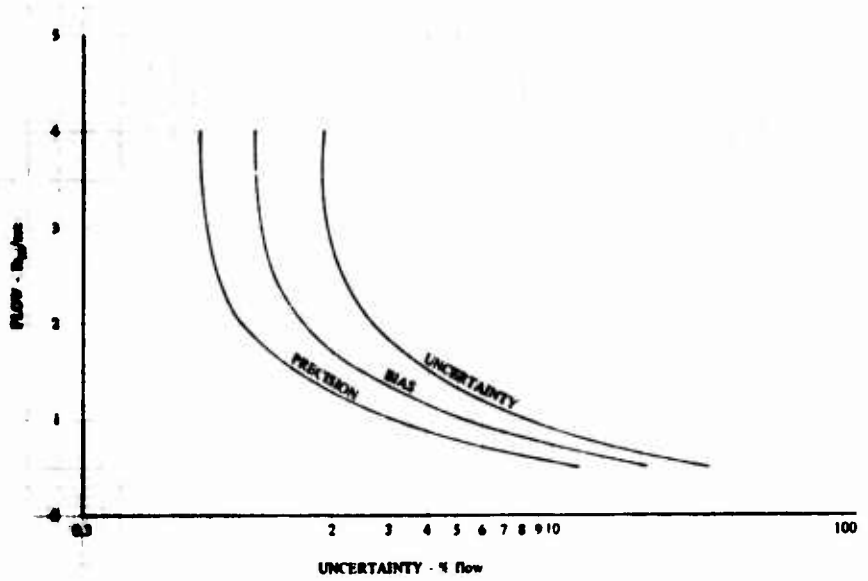

Figure 21. Inlet Orifice Flow Measurement Uncertainty.

As outlined in the data reduction procedures portion of Section V, inducer performance data were reduced using an IBM 370 streamline analysis program and, for the case of data to be compared with 10:1 program inducer performance, were also reduced by the IBM 1130 CCDRP program. As is shown in Figures 22 and 23, the inducer and impeller inlet conditions at 99% speed and 0-deg IGV calculated by each of these data reduction methods are in good agreement, especially near the hub and shroud walls. The slight differences noted near midspan are due mainly to the linear static pressure profiles input into the 1130 program that are compared to the static pressure profiles calculated by the streamline analysis program in Figures 24 and 25. It is felt that the streamline analysis program represents the more accurate description of the actual rig conditions.

TABLE 9. 99% SPEED, 0-DEG IGV, STEADY-STATE PRINTOUT

(Time Interval Beginning at 11530.125)

Header	Units	Channel	Averages	3x Sigma	Maximum	Minimum	Scans Used
PERFA1	PSID	0	-0.213	1.219	0.844	-1.165	19
SHORT1	CNTS	1	-0.053	0.688	0.0	-1.000	19
PSO-01	PSIA	2	14.719	0.024	14.737	14.706	19
PSO-02	PSIA	3	14.715	0.022	14.727	14.711	19
PSO-03	PSIA	4	14.715	0.029	14.731	14.700	19
APSO	PERF	5	14.716	0.016	14.726	14.711	19
PSOD-01	PSID	6	1.479	0.034	1.507	1.465	19
PSOD-02	PSID	7	1.485	0.060	1.523	1.442	19
PSOD-03	PSID	8	1.473	0.034	1.489	1.447	19
APSOD	PERF	9	1.479	0.027	1.497	1.465	19
TTP-01	DERT	10	534.396	0.245	534.582	534.270	19
TTP-02	DERT	11	534.236	0.302	534.506	534.087	19
TTP-03	DERT	12	534.641	0.323	534.836	534.518	19
TTP-04	DERT	13	534.564	0.316	534.741	534.426	19
TTP-05	DERT	14	534.743	0.330	534.926	534.610	19
ATTP	PERF	15	534.516	0.126	534.592	534.403	19
PTP-01	PSIA	16	13.479	0.019	13.496	13.464	19
PTP-02	PSIA	17	13.469	0.028	13.479	13.447	19
PTP-03	PSIA	18	13.473	0.024	13.481	13.465	19
APTP	PERF	19	13.474	0.018	13.480	13.459	19
TUTR-1	PERF	20	554.941	0.146	555.039	554.854	19
RT1-01	USID	21	1.099	0.006	1.101	1.097	19
TT1-01	PERF	22	585.830	2.361	587.134	584.438	19
RT1A01	USID	23	1.000	0.003	1.002	0.998	19
AA1A01	USID	24	53.252	0.214	53.366	53.106	19
PT1A01	PERF	25	20.741	0.194	20.879	20.663	19
TT1A01	PERF	26	706.335	0.600	706.584	705.931	19
BLANK		27	-5.105	2.212	-4.000	-6.000	19
BLANK		28	18.316	1.433	19.000	18.000	19
BLANK		29	60.263	1.357	61.000	60.000	19
PREF	PSIA	30	20.089	0.043	20.110	20.057	19
SVH-1	PERF	31	48.000	0.0	48.000	48.000	19
SVP-1	PSID	32	0.035	0.062	0.060	0.004	19
SVRP-1	PERF	33	16.089	0.072	16.127	16.047	19
SVH-2	PERF	34	48.000	0.0	48.000	48.000	19
SVP-2	PSIA	35	14.768	0.383	15.194	14.519	19
SVRP-2	PERF	36	16.108	0.423	16.571	15.835	19
SVTT1	PERF	37	540.708	0.877	541.376	540.349	19
SVTT2	PERF	38	536.949	0.910	537.472	536.441	19
BLANK	PERF	39	1.000	0.0	1.000	1.000	19
APSIS	PERF	40	12.286	0.0	12.286	12.286	19
APS1AS	PERF	41	20.922	0.0	20.922	20.922	19
APSIR	PERF	42	56.370	0.0	56.370	56.370	19
APS2S4	PERF	43	57.989	0.0	57.989	57.989	19
APS2H4	PERF	44	57.875	0.0	57.875	57.875	19
APS38	PERF	45	147.292	0.0	147.292	147.292	19
PS3-06	PERF	46	147.607	0.859	148.170	147.013	19
IGVACH	PERF	47	86.239	0.465	86.395	86.001	19

TABLE 9. 99% SPEED, 0-DEG IGV, STEADY-STATE PRINTOUT (Continued)

(Time Interval Beginning at 11530.125)

Header	Units	Channel	Averages	3x Sigma	Maximum	Minimum	Scans Used
BKFTM1	PERF	48	1049.103	7.928	1052.363	1043.363	19
TTSHRD	PERF	49	719.652	3.412	721.349	717.642	19
TT3-01	PERF	50	1143.463	1.215	1144.454	1142.610	19
TT3-02	PERF	51	1144.401	1.357	1145.015	1143.742	19
TT3-03	PERF	52	1146.558	1.307	1147.454	1145.614	19
TT3-04	PERF	53	1138.019	1.205	1138.952	1137.590	19
ATT3	PERF	54	1143.110	0.720	1143.661	1142.694	19
TTBLAC	PERF	55	1012.386	2.095	1013.705	1010.979	19
TTBAOR	DECA	56	682.521	0.676	682.740	682.089	19
PSBAOR	PSIA	57	52.134	0.167	52.287	52.075	19
DELPBA	PSID	58	0.034	0.076	0.092	-0.003	19
WACTBA	PERF	59	0.021	0.001	0.022	0.020	19
FCOXT1	PERF	60	636.377	0.662	636.832	636.195	19
FBBTM1	PERF	61	664.615	0.771	665.032	664.112	19
FRBTM1	DECA	62	633.184	0.642	633.694	632.779	19
RBTMP1	PERF	63	618.527	0.494	618.671	618.032	19
WACT	PERF	64	2.871	0.025	2.889	2.859	19
TR	PERF	65	2.204	0.001	2.205	2.203	19
SHUM	PERF	66	0.014	0.0	0.014	0.014	19
WCORBA	PERF	67	0.023	0.002	0.024	0.022	19
SPEED1	RPM	68	66152.687	197.822	66266.312	66086.500	19
SPEED2	RPM	69	66366.687	228.638	66468.937	66264.437	19
NCOR	PERF	70	65271.328	177.474	65340.254	65186.242	19
WCOR	PERF	71	3.179	0.028	3.199	3.164	19
WCORNT	PERF	72	3.156	0.029	3.177	3.140	19
PRST	PERF	73	10.044	0.058	10.082	10.004	19
TEFTTS	PERF	74	0.758	0.003	0.759	0.756	19
TEFNET	PERF	75	0.753	0.003	0.755	0.752	19
PRS	PERF	76	10.023	0.0	10.023	10.023	19
EFFTTS	PERF	77	0.757	0.001	0.757	0.756	19
EFFNET	PERF	78	0.752	0.001	0.753	0.752	19
EFFHUM	PERF	79	0.762	0.001	0.763	0.761	19
AMPRES		80	14.715	0.0	14.715	14.715	19
TWET		81	69.000	0.0	69.000	69.000	19
TDRY		82	76.000	0.0	76.000	76.000	19

NOTE: All efficiencies are calculated based on inlet plenum average temperature.

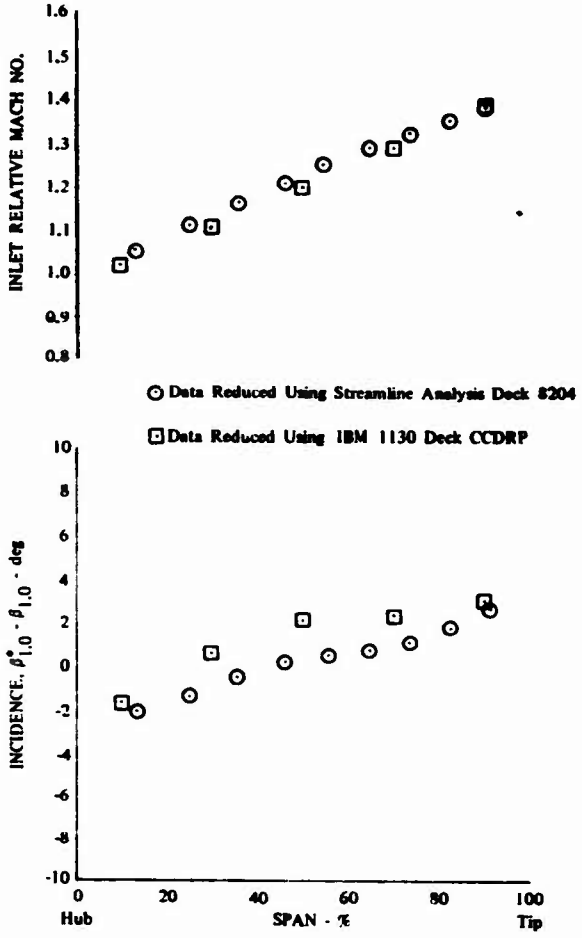

Figure 22. Data Reduction Method Comparison of Inducer Inlet Conditions at 99% Speed and 0-deg IGV.

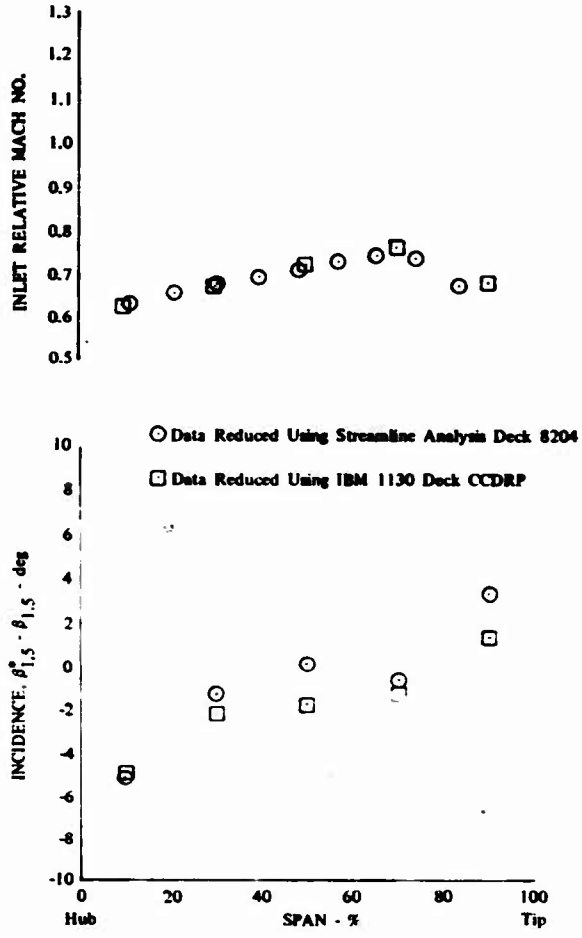

Figure 23. Data Reduction Method Comparison of Impeller Inlet Conditions at 99% Speed and 0-deg IGV.

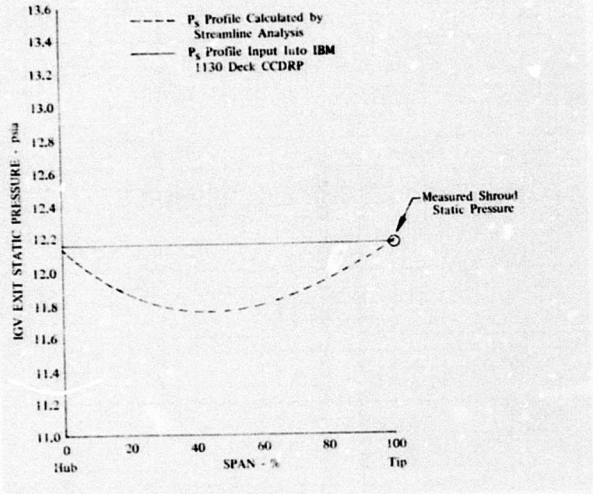

Figure 24. IGV Exit Static Pressure Profile at 99% Speed and 0-deg IGV.

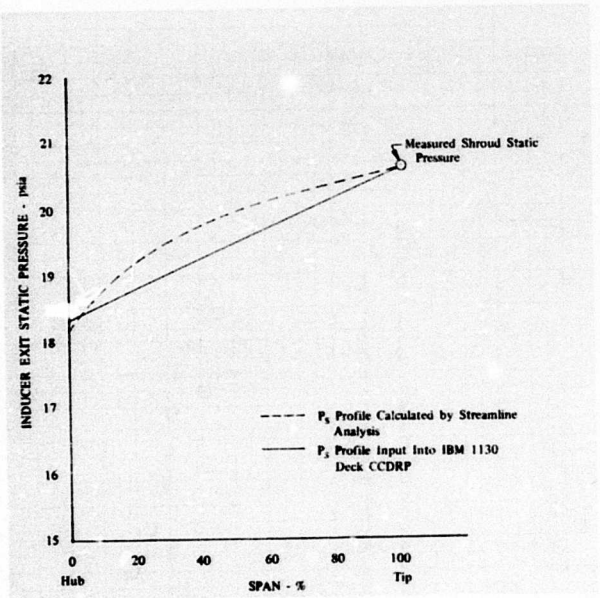

Figure 25. Inducer Exit Static Pressure Profile at 99% Speed and 0-deg IGV.

SECTION VII

RESULTS AND DISCUSSION

OVERALL PERFORMANCE

The overall performance map is presented in Figure 26, and a complete tabulation of overall performance data is listed in Table 10. As can be seen in Figure 26, the design speed performance surpassed the original 10:1 program goals of 10:1 pressure ratio (total-to-static) and 75% efficiency. At 99% design speed and 0-deg inlet guide vane setting, the surge pressure ratio is 10:07:1 at a corresponding peak efficiency of 78.4%.

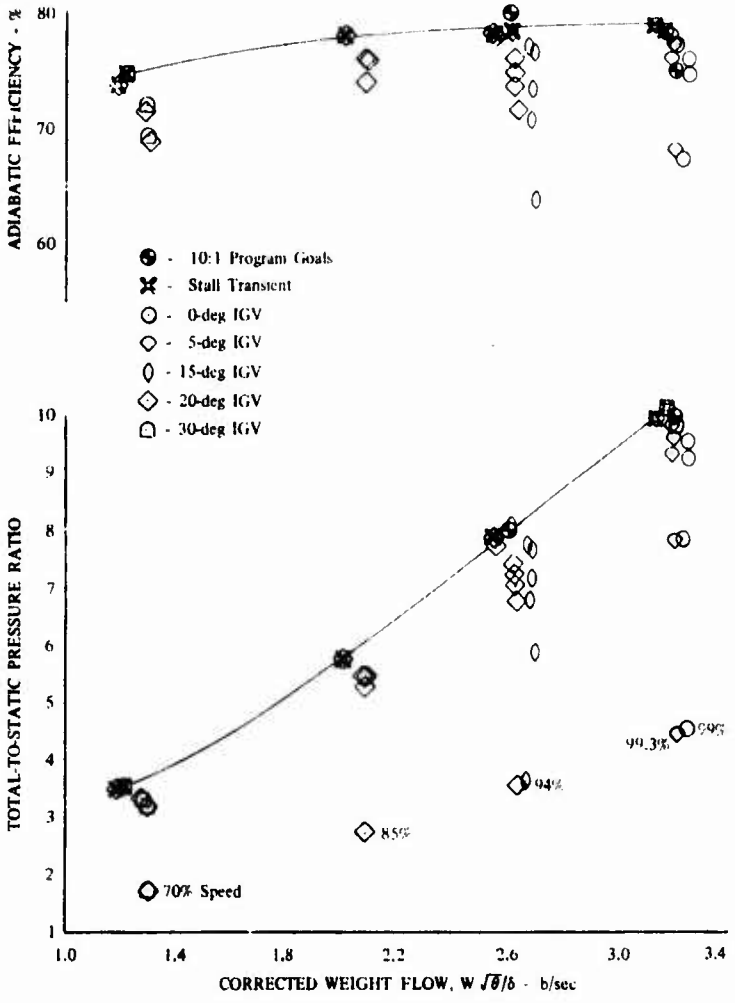

Figure 26. Overall Performance.

SECTION VII

RESULTS AND DISCUSSION

OVERALL PERFORMANCE

The overall performance map is presented in Figure 26, and a complete tabulation of overall performance data is listed in Table 10. As can be seen in Figure 26, the design speed performance surpassed the original 10:1 program goals of 10:1 pressure ratio (total-to-static) and 75% efficiency. At 99% design speed and 0-deg inlet guide vane setting, the surge pressure ratio is 10:07:1 at a corresponding peak efficiency of 78.4%.

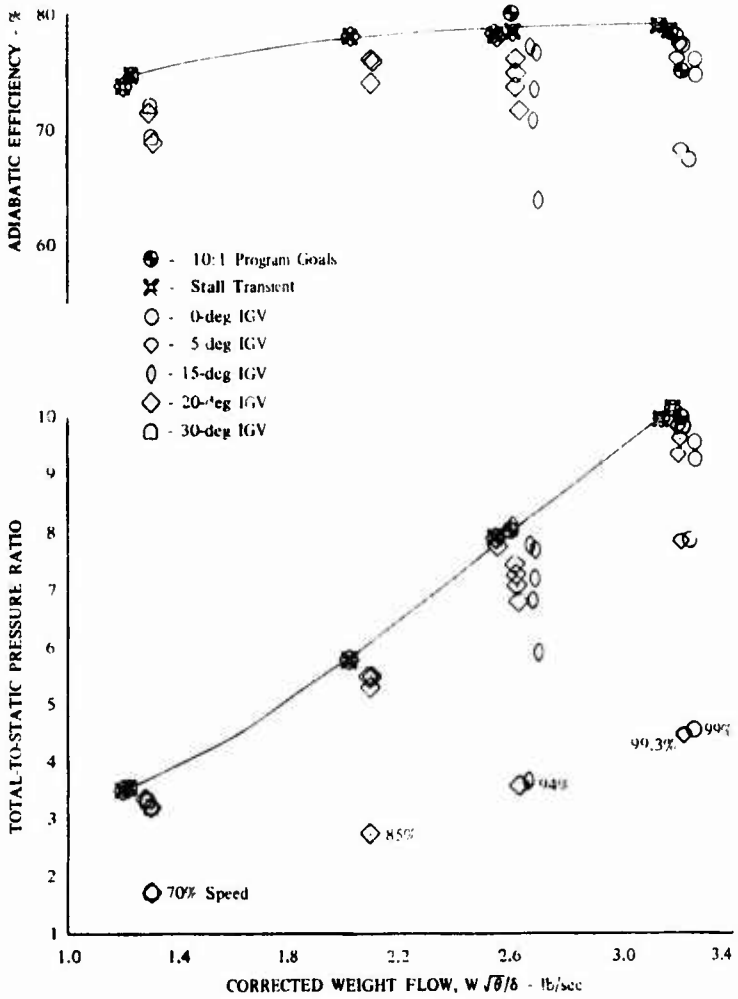

Figure 26. Overall Performance.

TABLE 10. OVERALL PERFORMANCE TABULATION*

Speed, %	IGV, Setting, deg	Net Weight Flow, lb_m/sec	Pressure Ratio (Total-to-Static)	Net Efficiency (Total-to-Static)
70	30	1.228	3.544	0.747
		1.295	3.341	0.719
		1.306	3.208	0.693
		1.313	1.765	0.309
85	20	2.028	5.781	0.781
		2.097	5.490	0.760
		2.105	5.488	0.759
		2.102	5.299	0.740
		2.099	2.755	0.407
94	15	2.612	8.077	0.783
		2.671	7.764	0.771
		2.690	7.673	0.765
		2.680	6.789	0.706
		2.684	7.186	0.733
		2.695	5.859	0.637
		2.667	3.638	0.432
	20	2.548	7.827	0.783
		2.553	7.736	0.780
		2.621	7.436	0.761
		2.622	7.257	0.749
		2.622	7.080	0.737
		2.631	6.785	0.716
		2.638	3.567	0.431
99	0	3.170	10.067	0.784
		3.205	9.832	0.773
		3.249	9.582	0.761
		3.249	9.285	0.747
		3.240	7.851	0.673
		3.250	4.555	0.450
99.1	0	3.171	10.090	0.785
		3.204	10.023	0.782
		3.197	9.940	0.778**
		3.266	9.721	0.768**
		3.194	9.853	0.774**
		3.265	9.698	0.767**
		3.197	9.853	0.774**
		3.268	9.558	0.760**

TABLE 10. OVERALL PERFORMANCE TABULATION*
(Continued)

Speed, %	IGV, Setting, deg	Net Weight Flow, lb_m/sec	Pressure Ratio (Total-to-Static)	Net Efficiency (Total-to-Static)
99.3	5	? .0	9.949	0.790
		[illegible]	9.835	0.783
		3.198	9.604	0.773
		3.188	9.336	0.7596
		3.198	7.840	0.6812
		3.213	4.481	0.4553
99.4	0	3.234	10.219	0.783
		3.248	10.097	0.777
		3.263	9.992	0.773
		3.286	9.831	0.765
		3.271	4.599	0.455

*Data obtained at sea level inlet conditions and calculated with variable specific heat ratio.

**With impeller exit bleed flow in sets of stall transient and near stall steady-state points with increasing bleed.

The relatively flat efficiency characteristic climbs slowly from 75% speed to design speed. The overall peak efficiency of 79% occurs at 99.3% speed and 5-deg IGV setting at a pressure ratio of 9.95:1.

Overall performance data, which has been corrected to the plenum total temperature for comparison with 10:1 program performance, is presented in Figure 27, along with the peak efficiency and pressure ratio surge lines attained with the same inlet configuration in the 10:1 program, and shows the benefit of the new inducer and diffuser. The apparent increase in low-speed surge pressure ratio actually is caused by decreased flow rate set by the smaller modified diffuser throat area.

The slight decrease in demonstrated efficiency at 8:1 pressure ratio is potentially also a result of this smaller throat area. Internal performance calculations show that the diffuser was matched to allow peak efficiency at approximately 8:1 pressure ratio in the 10:1 program. The smaller area and the apparent match at 10:1 pressure ratio in this program most likely caused the slight efficiency change by preventing the inducer-impeller from operating at its optimum point at 8:1 pressure ratio.

When presented as surge pressure ratio vs corrected speed, as in Figure 28, the Modified Centrifugal Compressor surge line is essentially matched by that of the 10:1 program at low speed but exceeds the 10:1 program surge line where the original inducer was operated above its design speed and at a lower prewhirl than anticipated.

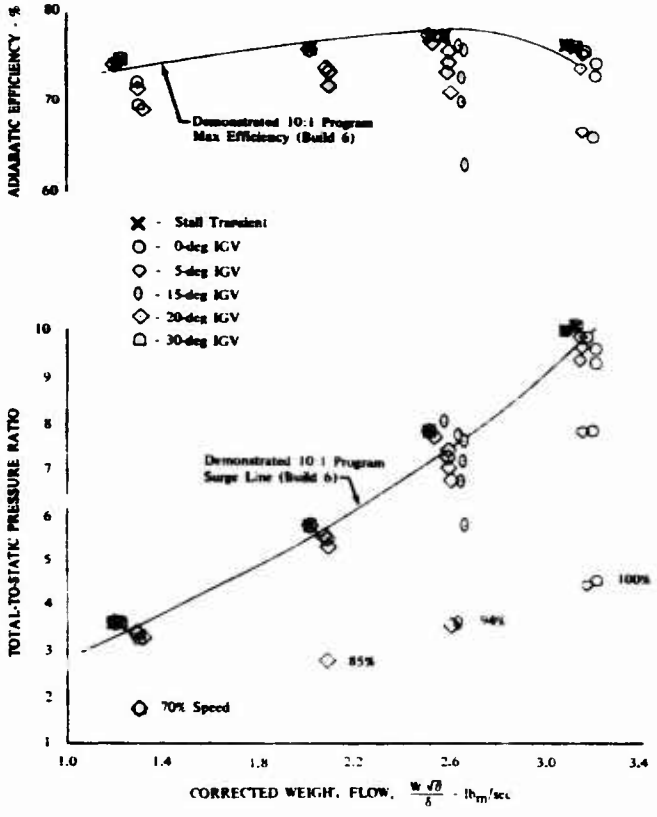

Figure 27. Overall Performance Comparison (Efficiency Calculated Using Plenum Temperature Ignoring Preheating Effect).

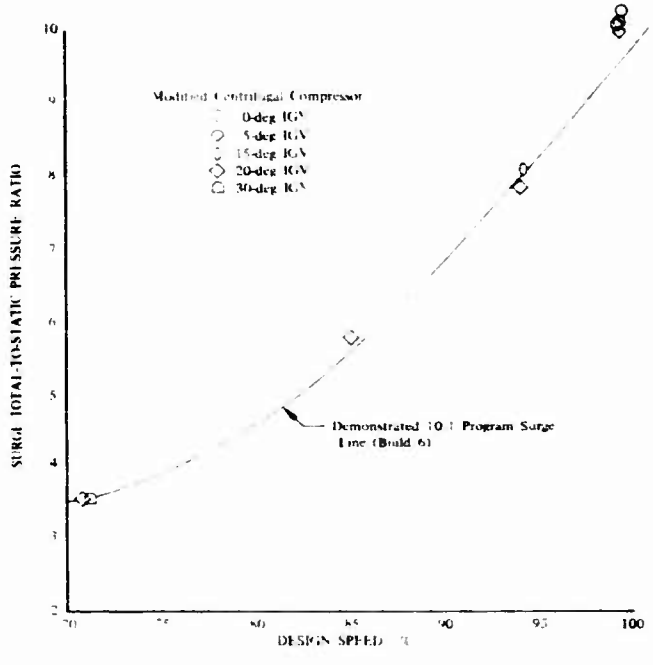

Figure 28. Surge Pressure Ratio Comparison of the Modified Centrifugal Compressor and the 10:1 Program.

The 99% speed and 0-deg prewhirl efficiency was not improved by activating the shroud side impeller exit bleed. Pressure ratio fell off as the bleed was increased, indicating that overall performance suffered as additional flow through the inducer caused losses to increase as if the inducer were operating at a "choked" incidence.

Very low-speed overall pressure ratio vs weight flow is presented in figure 29 at 30% of design speed for 30- and 40-deg inlet guide vane settings. Surge was not abrupt at these conditions and is estimated based upon inspection of all available data during these traverses. The surge was not easily detected on the test stand at these conditions, as the compressor pressure ratio remained reasonably stable after the orifice instrumentation had indicated reversed flow. Efficiency was not calculated for these low-speed data, as they were obtained after extended high-speed running, which completely heated the inlet, and no temperature traverses were available to allow determination of real temperature ratio.

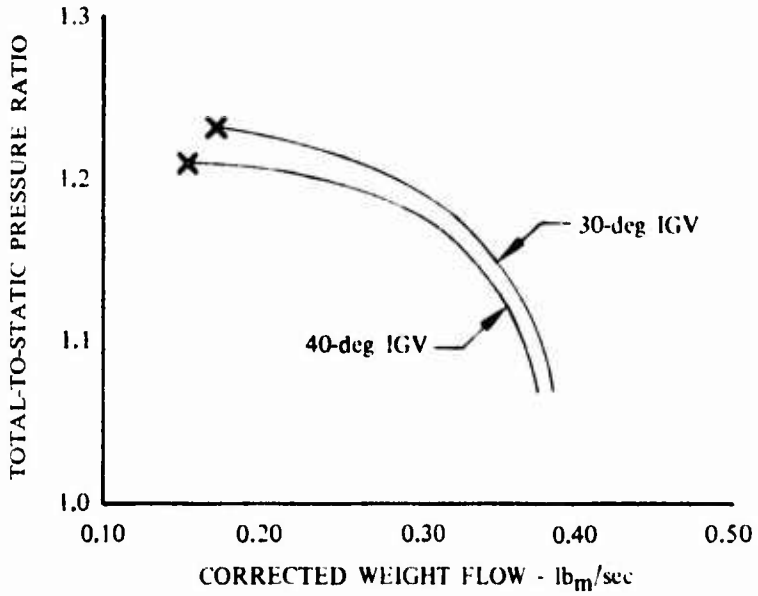

Figure 29. Pressure Ratio Characteristics at 30% Speed.

The choke point flow comparison presented in Figure 30 also indicates that the smaller diffuser throat passes less flow than the 10:1 program diffuser at low speed, but near design speed the higher pressure rise of the modified configuration creates greater flow at the same condition. The continuing rise in flow at approximately design speed as prewhirl was decreased indicates that the flow was never absolutely choked in the area of the inducer.

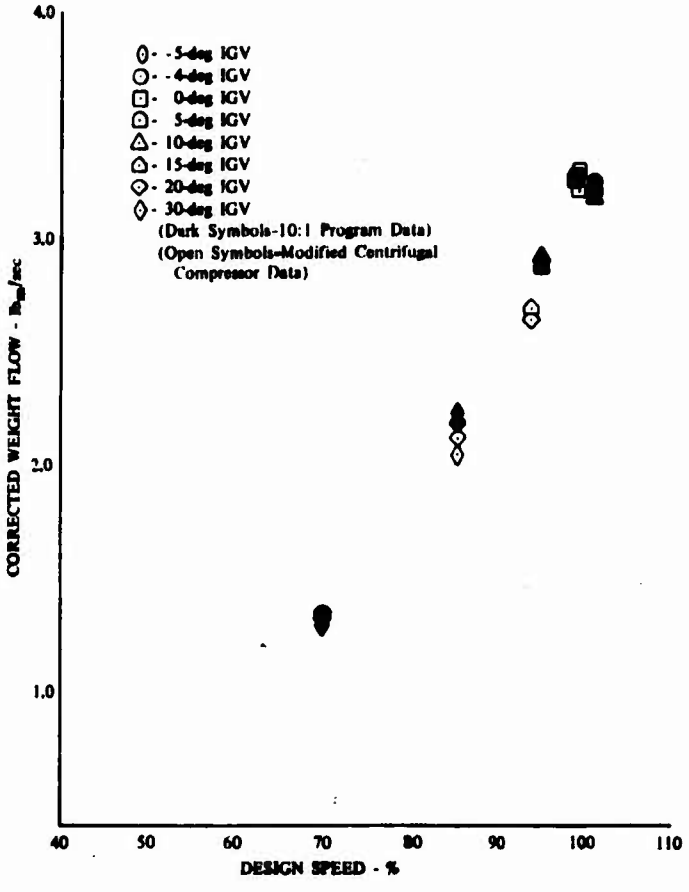

Figure 30. Choke Point Flow Comparison.

INLET GUIDE VANE TEMPERATURE TRAVERSES

Inlet guide vane exit radial temperature traverses, as described in this report and obtained by the temperature probe shown in Figure 16, were used to determine the inlet temperature used for temperature ratio in both overall and component performance calculations. These temperature traverses were obtained as a result of observation of apparent inlet temperature gradients upstream of the inducer in the 10:1 program, indicating that the air near the shroud was considerably hotter than that of the plenum. Circumferential traverses also revealed that the regions behind the struts (which were used for supply and scavenge of the front bearing compartment lubricating and cooling oil) and guide vanes were even hotter than the mid-vane positions of the radial traverses. These observations, along with rig case thermocouple data obtained during the mechanical checkout of the redesigned rig during the 10:1 program, indicate that the inlet cases were surprisingly hot. Reverse flow from the inducer was discounted since air angle and total pressure data (also recorded simultaneously) did not exhibit this characteristic, although low-speed (70%) IGV traverses did. The

reverse flow characteristics were obvious and very different from the temperature gradients observed. Inlet case temperatures continued to rise after complete rig shutdowns, which also led to the conclusion that secondary flows from the inducer were not responsible.

A very accurate and responsive traverse probe was constructed and used to measure these temperature gradients for this program. The resultant radial temperature traverses are shown in Appendix A. These traverses were obtained out of the hot wakes observed in the 10:1 program data to be conservative, and the profiles were nearly the same as seen in the previous 10:1 program data. The apparent accuracy of the probe is substantiated, as the free-stream temperatures reach the corrected standard day plenum temperature. Response of the probe is such that temperature changes of approximately 100 deg were sensed in the same 0.1 sec that the other instrumentation signaled that a surge had occurred.

An analysis of the heat transfer necessary to cause the levels of inlet preheating and the potential heat transfer paths observed from hot regions of the diffuser collector and turbine has not fully substantiated the experimentally measured heat input. However, temperatures of up to 700°R have been recorded by the inlet probe withdrawn into the wall but not in contact with any metal during the present test.

COMPONENT PERFORMANCE

The performance map for the modified inducer is presented in Figure 31, and the modified inducer performance data are listed in Table 11. The inducer performance fell slightly below its predicted design pressure ratio of 1.924:1 and 92% efficiency at 3.2 lb of flow. At 99% speed and 0-deg IGV, the modified inducer obtained a pressure ratio of 1.886 at an efficiency of 87.22% and 3.205 lb of flow. The actual characteristics of the inducer with speed at a constant inlet guide vane setting are difficult to determine due to the inlet guide schedule used in this test; however, trends are distinguishable. The high-speed, 0-deg data seem to indicate that the inducer is operating on the choke or negative incidence angle side of its characteristic. This trend was observed on the test stand when the 20-deg inlet guide vane point at 2.62 lb of flow was obtained. During the traverse, the rig stalled and the point was reset slightly down the speed line. The absolute pressure level of the new inducer traverse point was also reduced, indicating that the inducer characteristic was steep at this point.

The losses of the modified inducer calculated using the measured inlet and exit profiles, as described in the inducer performance section, are compared to the design loss distribution in Figure 32. The measured losses are slightly higher than those predicted over most of the span, with a rapid increase in the measured losses relative to the prediction occurring near the shroud wall. These loss levels are compatible with the inducer performance data, which showed that the inducer was not up to design pressure ratio and efficiency at this condition. Loss distributions of the original 10:1 program inducer are also presented in Figure 32 for comparison. The losses of the modified inducer are slightly lower across the span as compared to the original when each is operating at its particular design condition, even though it produces a considerably higher pressure ratio. The original inducer was designed to accept 10 deg of prewhirl, and the modified

inducer was designed to accept 0 deg of prewhirl. The improvement produced by the inducer modification is demonstrated by the significant decrease in losses of the modified inducer relative to the losses shown for the 10:1 program inducer when subjected to the conditions required during that program to produce an overall compressor pressure ratio of 10:1 (101% speed, -4-deg inlet guide vane setting). A comparison of the modified and original inducer performance, both reduced using the same data reduction system as used in the 10:1 program, is presented in Figure 33. As expected, a significant improvement in the performance for the modified inducer is shown at design flow.

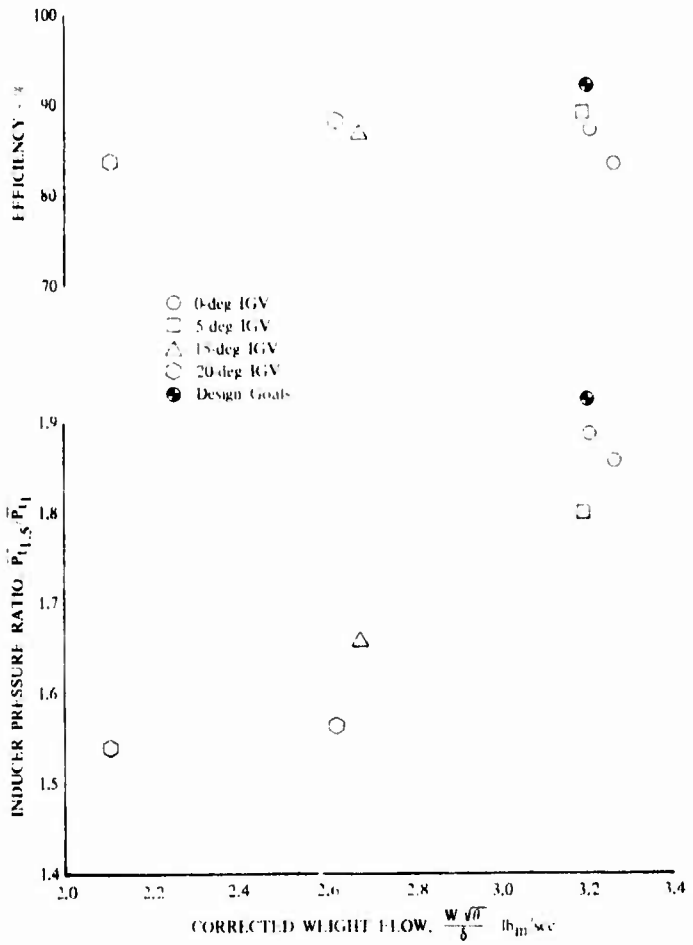

Figure 31. Modified Inducer Performance.

TABLE 11. MODIFIED INDUCER PERFORMANCE

(REDUCED USING STREAMLINE ANALYSIS DECK 8204)

Speed, %	IGV Setting, deg	Weight Flow, lb_m/sec	Pressure Ratio	Efficiency, %
85	20	2.105	1.539	83.78
94	15	2.671	1.658	86.79
94	20	2.621	1.564	88.25
99	0	3.205	1.886	87.22
99.3	5	3.190	1.800	89.19
99.4	0	3.263	1.857	83.45

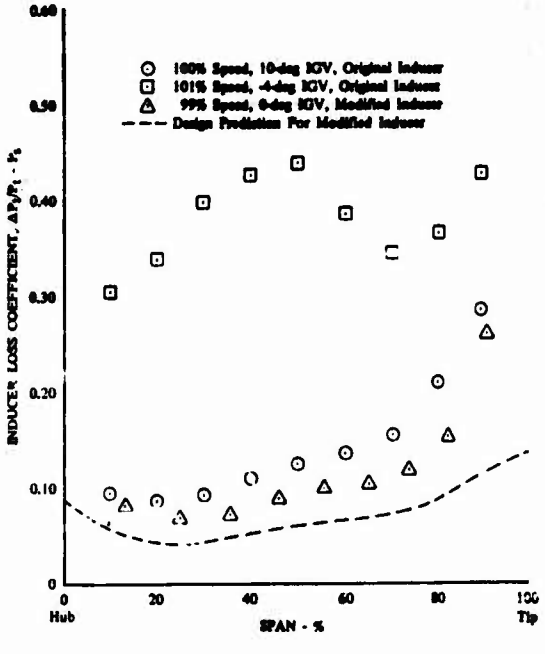

Figure 32. Inducer Loss Comparison.

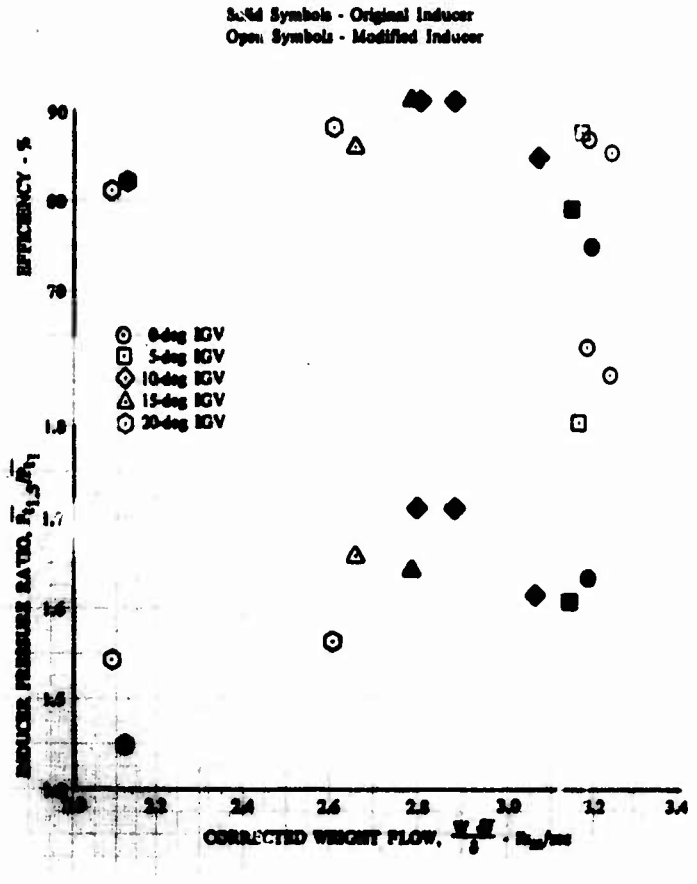

Figure 33. Inducer Performance Comparison (Reduced Using Inlet Plenum Temperature Instead of Inlet Traverses for Comparison).

The inducer performance was also analyzed by comparing the design work split and total work of the impeller and inducer with that obtained by internal flow data analysis. Assuming the same impeller inlet conditions as in the 10:1 program, the impeller was expected to produce a pressure ratio of 6.65:1 and a temperature ratio of 1.815:1. Calculating combined inducer-impeller conditions at the design point from test data results in a total rotor pressure ratio of 12.08 at a temperature ratio of 2.157. Subtracting the measured inducer performance would leave an impeller pressure ratio of 6.405 at a temperature ratio of 1.757, which approximates the expected performance based on the assumption of constant work in the impeller in both the modified and original configurations.

The inducer inlet relative Mach number and spanwise distributions of incidence angle at design conditions and at 99% speed and 0-deg IGV setting, reduced by the streamline analysis method, are shown in Figure 34. The choked incidence relative to design can be attributed to the slightly lower speed of the measured point. Comparable data, reduced in common with build 6 of the 10:1 program, are shown in Figure 35. The modified inducer ran more choked than at either the 10:1 program design point or the 10:1 program condition required to obtain 10:1 pressure ratio. The choked incidences exhibited in these figures by the modified inducer are also compatible with the inducer performance and loss data.

The inlet and exit air angle distributions and resulting turning are shown in Figure 36. The inducer inlet and exit relative air angles are both slightly high due to the underspeed of the reduced point, but resultant turning is very close to design, as the inducer overturned at the hub and underturned at the tip by a few degrees.

Inducer exit total pressure, air angle, and total temperature traverse data are presented in Appendix A for all data points recorded.

Impeller inlet conditions generated by the modified inducer at 99% speed and 0-deg inlet guide vane setting are shown in Figure 37, along with the design distribution. Inlet relative Mach number level and distribution were much as expected, except for the reduced Mach number caused by the previously noted higher-than-design inducer losses at the tip. The impeller leading-edge incidence is significantly more choked (6.5 deg at 10% span) than design at the hub. This difference decreases as the tip is approached, until at 90% span from the hub the design incidence is nearly matched. We must assume that the incidence change must have resulted in increased impeller losses. The impeller inlet conditions are compared in Figure 38 with 10:1 program data, reduced by the same method as in the 10:1 program. The impeller inlet relative Mach number is considerably reduced in the modified configuration over the span; however, the modified inducer created a more choked inlet condition to the impeller.

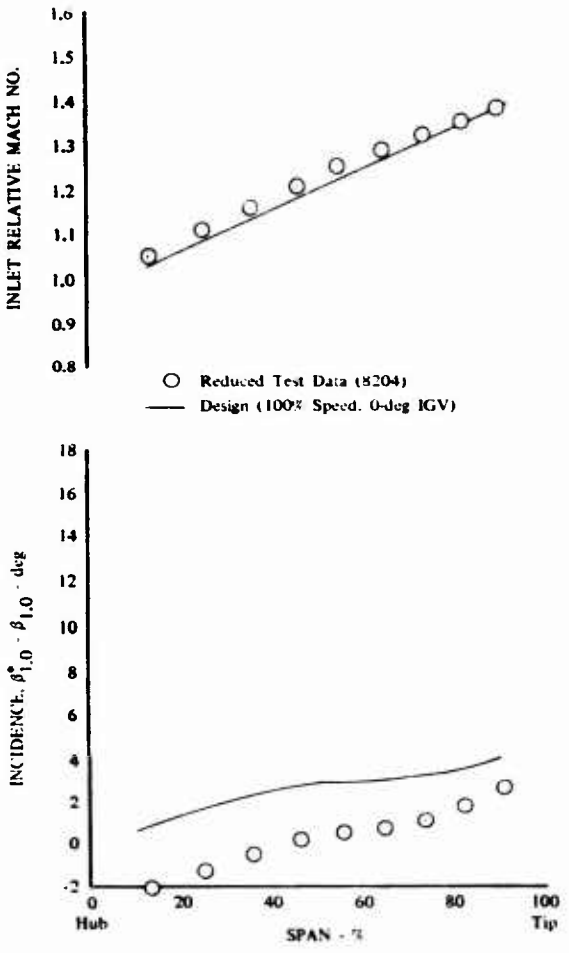

Figure 34. Inducer Inlet Conditions at 99% Speed and 0-deg IGV.

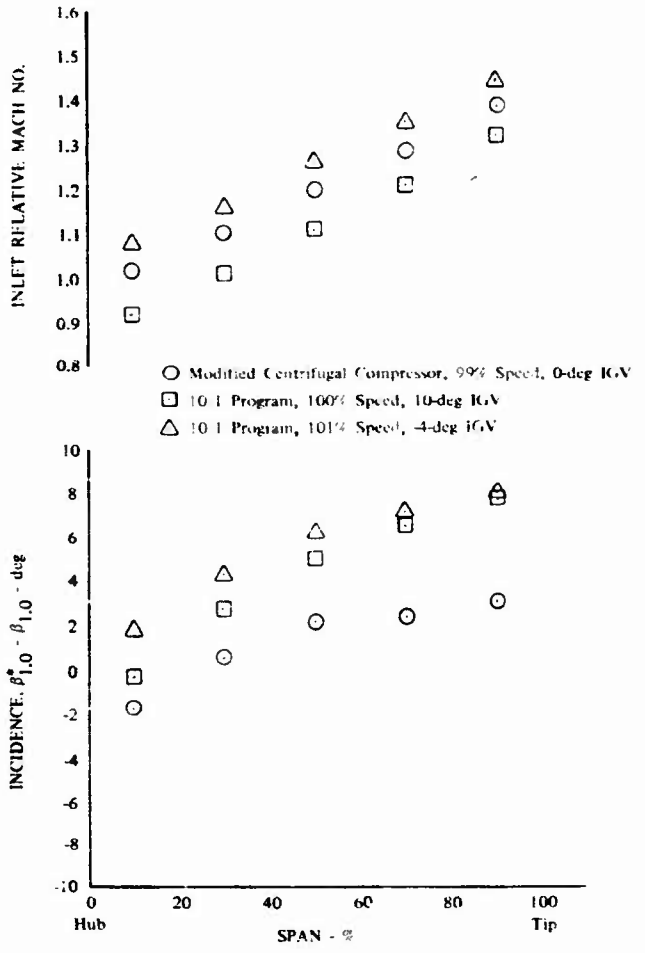

Figure 35. Inducer Inlet Conditions Comparison.

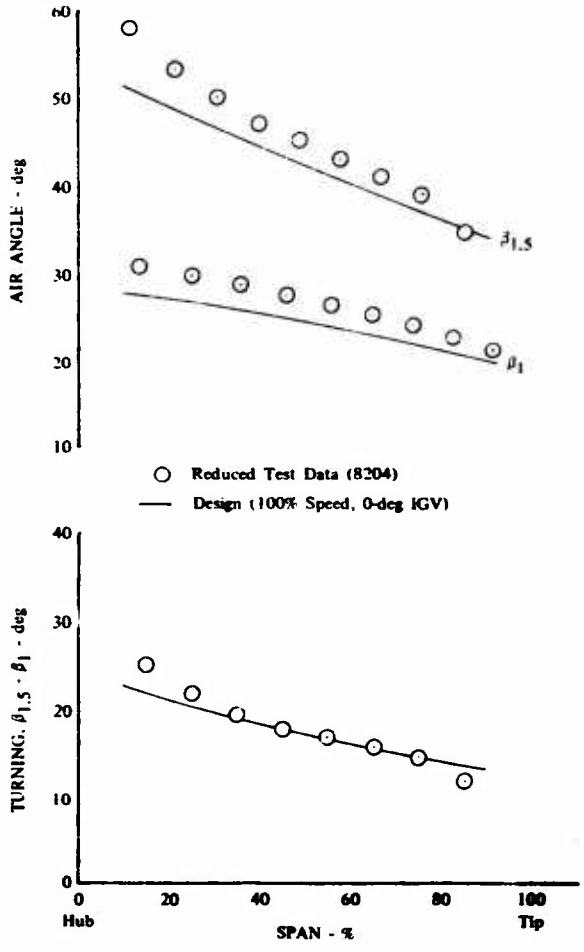

Figure 36. Inducer Exit Air Angle Profile at 99% Speed and 0-deg IGV.

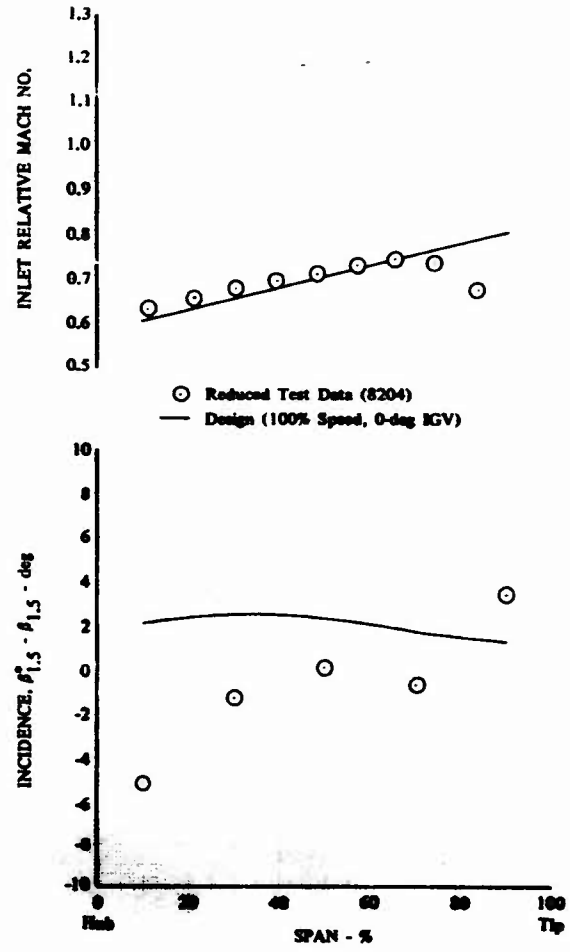

Figure 37. Impeller Inlet Conditions at 99% Speed and 0-deg IGV.

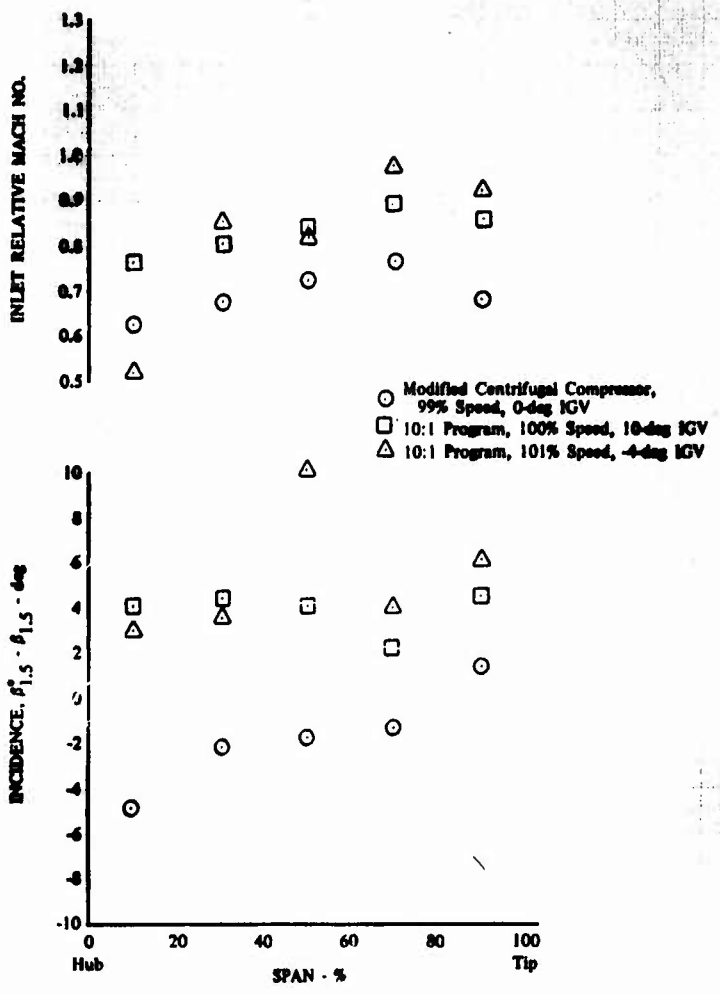

Figure 38. Impeller Inlet Conditions Comparison.

SECTION VIII

CONCLUSIONS

The program objective of improving the performance of the 10:1 pressure ratio single-stage centrifugal compressor as a result of modifications to the inducer was achieved. An efficiency of 78.4% was obtained at 10.07:1 total-to-static pressure ratio. This is 3.4 points greater than the design goal and has verified that high-pressure-ratio, high-efficiency, single-stage centrifugal compressors can be developed.

The successful modification to the inducer shows that transonic fan design technology can be used in other applications. The inducer performance also demonstrates the use of rugged, low-aspect blading in order to operate efficiently at higher blade loadings.

The sensitivity of the performance to diffuser sizing was demonstrated by the slight loss in efficiency at the 8:1 pressure ratio condition due to the diffuser size required to match at the design point.

This program was conducted with freedom from mechanical difficulty throughout the entire test sequence, and complete performance data were obtained. Axial impeller-to-shroud clearance was 0.001 in. at design speed (65,300 rpm), but no rub occurred and vibrations remained low throughout the test. The available horsepower of the test rig permitted the test to be conducted at sea level inlet conditions, eliminating the need for Reynolds number corrections to the measured performance.

SECTION IX

RECOMMENDATIONS

This test program has demonstrated the performance capability of a high-pressure-ratio, single-stage centrifugal compressor; however, analysis of this information has resulted in the following recommendations to define and improve the performance of simplified compressors for small gas turbine engines:

1. Now that the original design performance goal of 75% efficiency at a total-to-static pressure ratio of 10:1 has been surpassed, means for improvement of the range characteristics should be examined so that this performance potential can be of greater benefit in engine or gas generator applications. The impeller exit/diffuser entrance region is apparently the area that has the greatest influence on the range from choke to surge, but no effort to investigate this area or to increase the flow range was included in this limited-effort program. Thus, it is recommended that research be conducted to determine the factors influencing range, and that these results be used to provide a demonstration of improved range or surge margin by application of this information.

2. The slight loss in efficiency from the 10:1 program at 8:1 pressure ratio as a result of accurate diffuser matching at the 10:1 pressure ratio design condition points out the sensitivity of the compressor to small changes in diffuser geometry. This area should be more fully investigated and techniques or devices developed to allow adaptive matching or alleviation from the present sensitivity in order to develop optimum performance over a greater operating envelope. Even though the diffuser was accurately sized for the design condition in this program, the sensitivity of performance to diffuser size would make it advisable to modify the test rig so that diffuser changes can be made in the test mount without extensive disassembly and reassembly requirements.

3. Inlet preheating measurements obtained in this program demonstrate the need for more investigation into the effect of environment and configuration on apparent rig performance. Metal and air temperatures should be measured in future programs to allow further definition of any tendency of test configuration or extraneous sources to influence performance calculations. Data should be obtained to create standard or baseline performance, and environmental or operational conditions should be estimated and applied to this standard performance for gas generator or engine studies.

APPENDIX A

TRAVERSE DATA

Plots of inlet guide vane exit total temperature traverse data (Figures A-1 through A-6) and inducer exit total pressure, air angle, and total temperature traverse data (Figures A-7 through A-12) are presented. Total pressure and total temperature are ratioed to standard day plenum conditions but are otherwise uncorrected. Inlet guide vane exit total temperature traverses recorded at 94% speed, Figures A-2 and A-3, were obtained with the traverse probe in an inlet guide vane wake and were not used in performance calculations. The temperature sensor on the inducer exit traverse probe is offset 0.045 in. from the pressure sensing ports. Both the inlet guide vane exit and inducer exit traverse probes were stopped prior to the hub wall and traversed into recesses in the shroud wall.

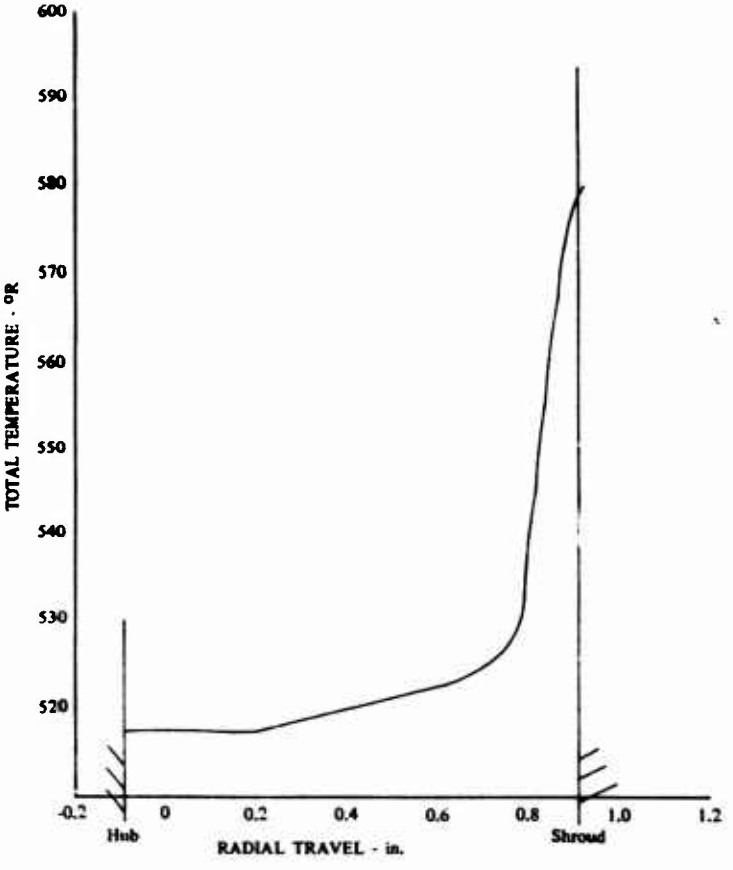

Figure A-1. IGV Exit Total Temperature Profile; 85% Speed, 20-deg IGV.

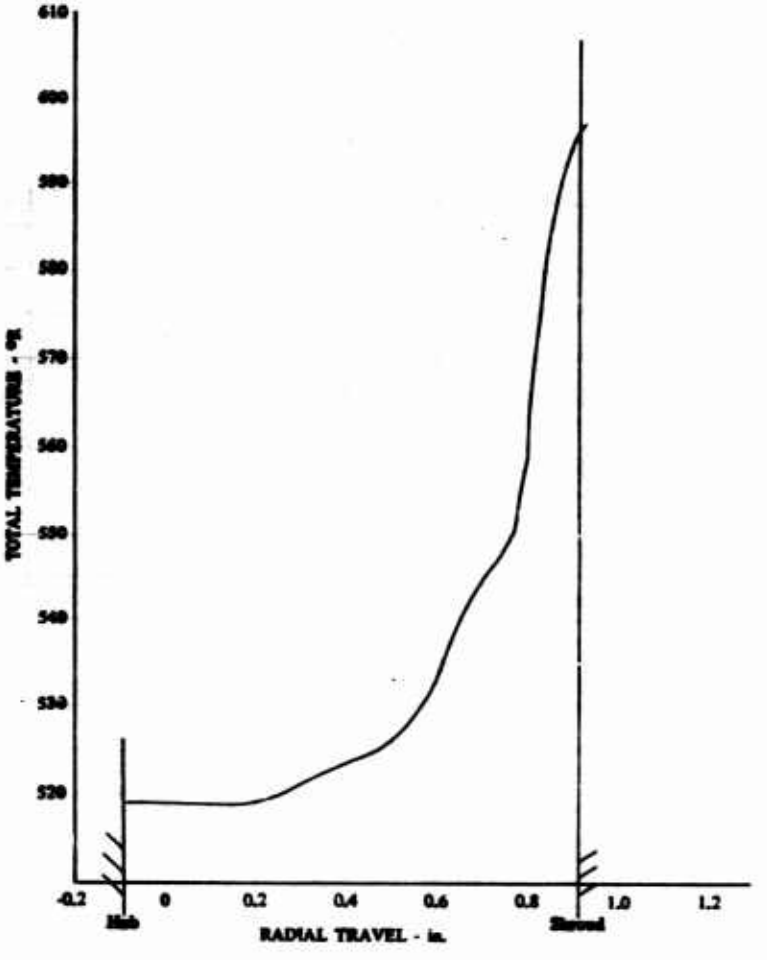

Figure A-2. IGV Exit Total Temperature Profile; 94% Speed, 15-deg IGV (Data Obtained With Probe Partially in an IGV Wake).

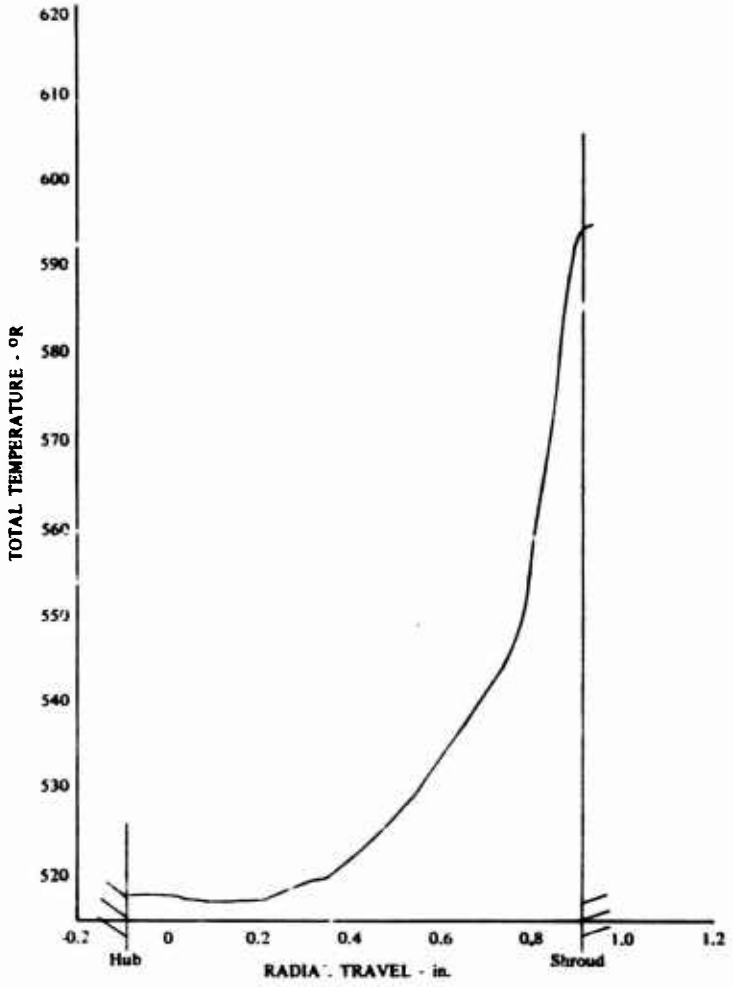

Figure A-3. IGV Exit Total Temperature Profile; 94% Speed, 20-deg IGV (Data Obtained With Probe Partially in an IGV Wake).

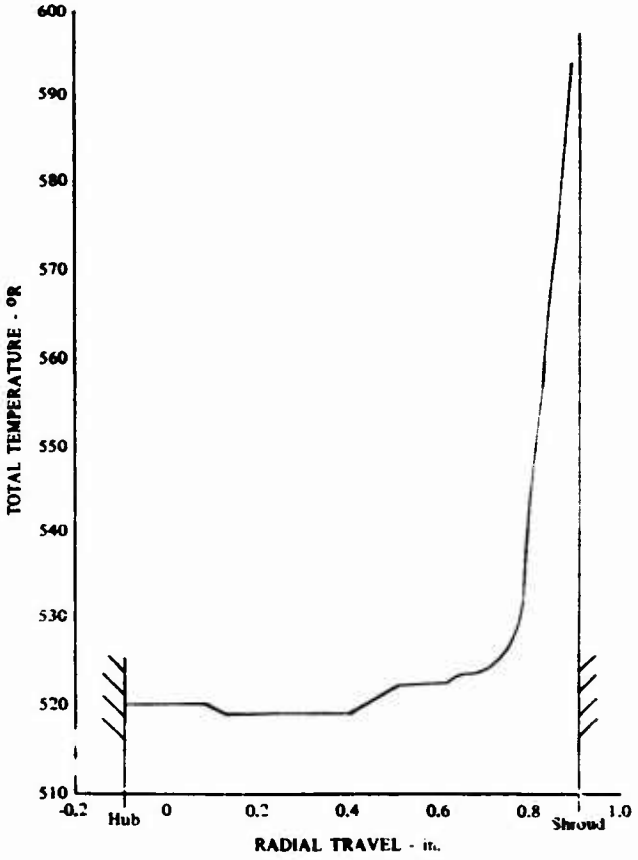

Figure A-4. IGV Exit Total Temperature Profile; 99% Speed, 0-deg IGV.

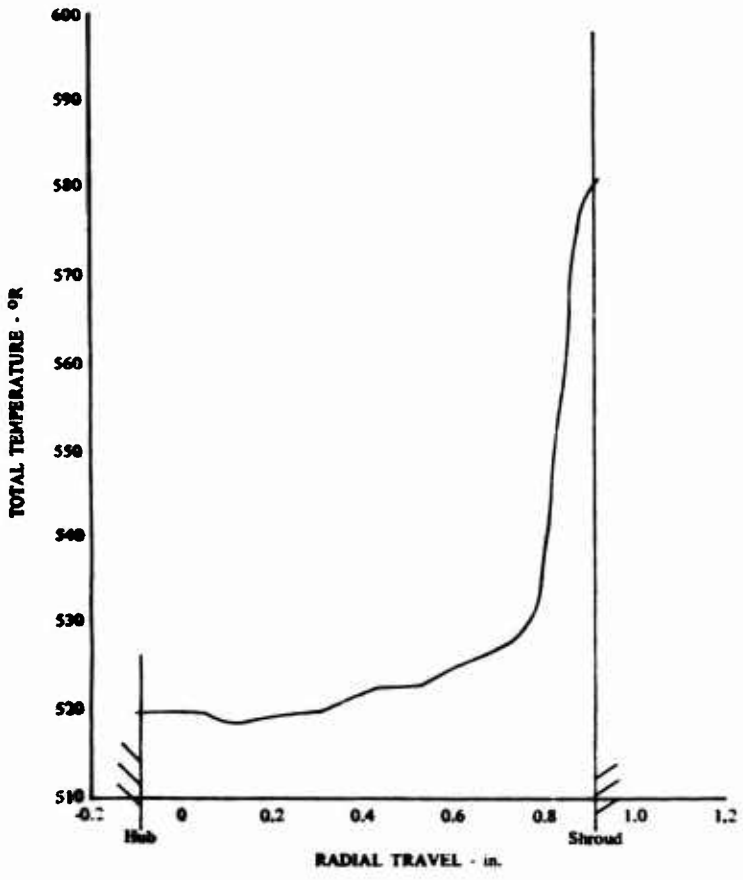

Figure A-5. IGV Exit Total Temperature Profile; 99.3% Speed, 5-deg IGV.

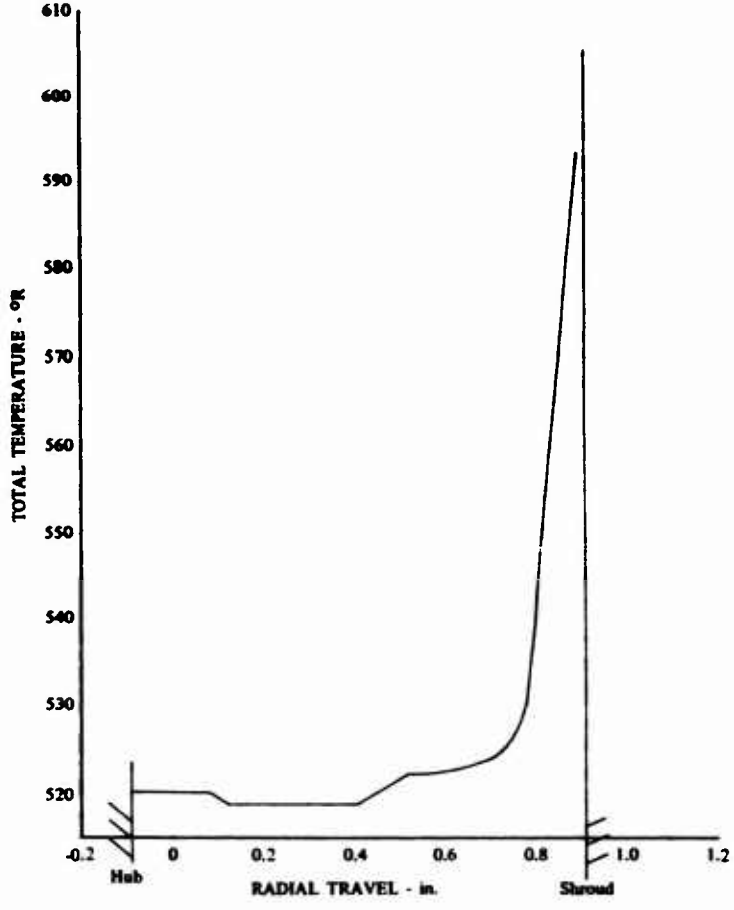

Figure A-6. IGV Exit Total Temperature Profile; 99.4% Speed, 0-deg IGV.

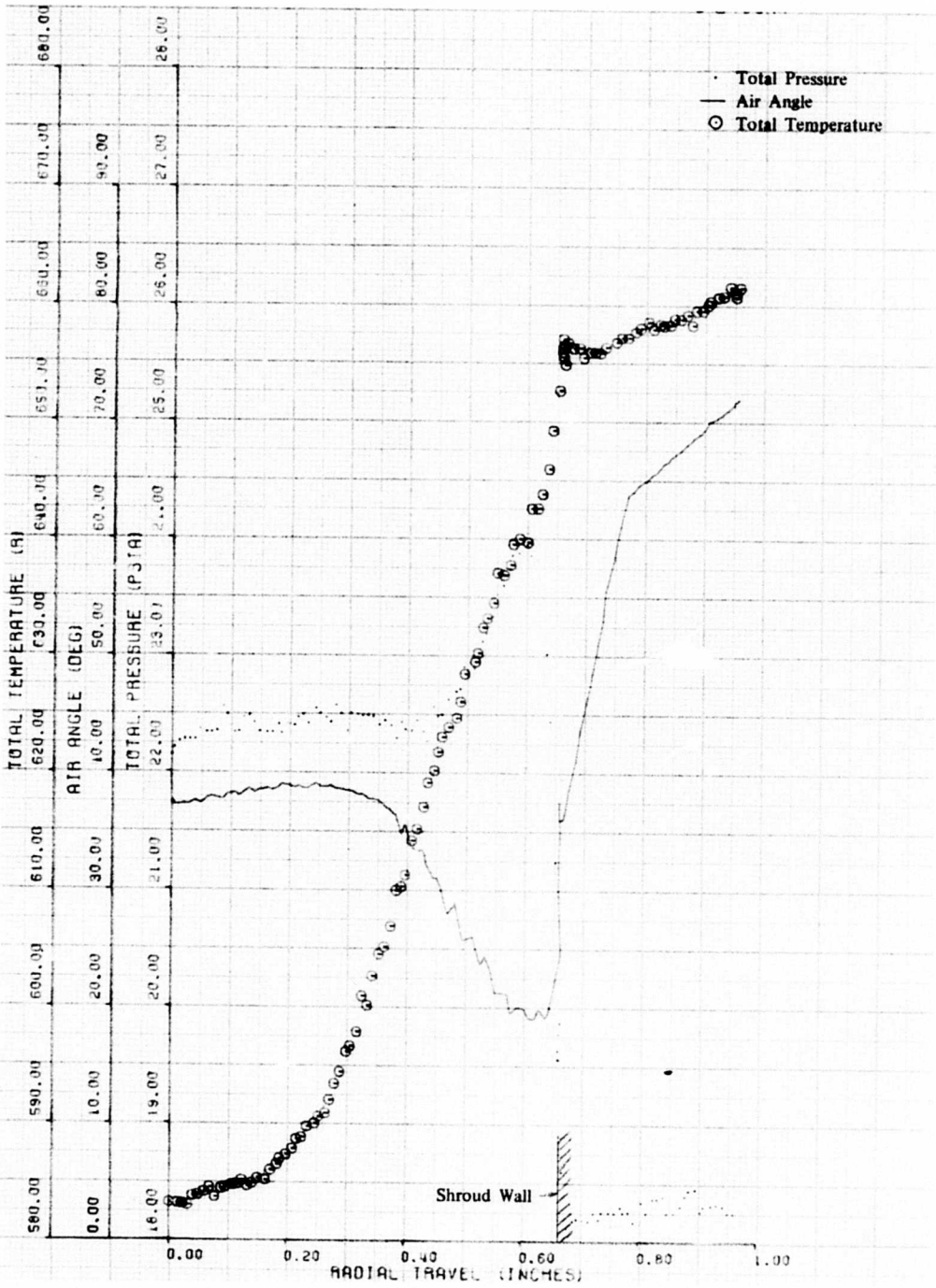

Figure A-7. Inducer Exit Traverse; 85% Speed, 20-deg IGV, Run 9.02.

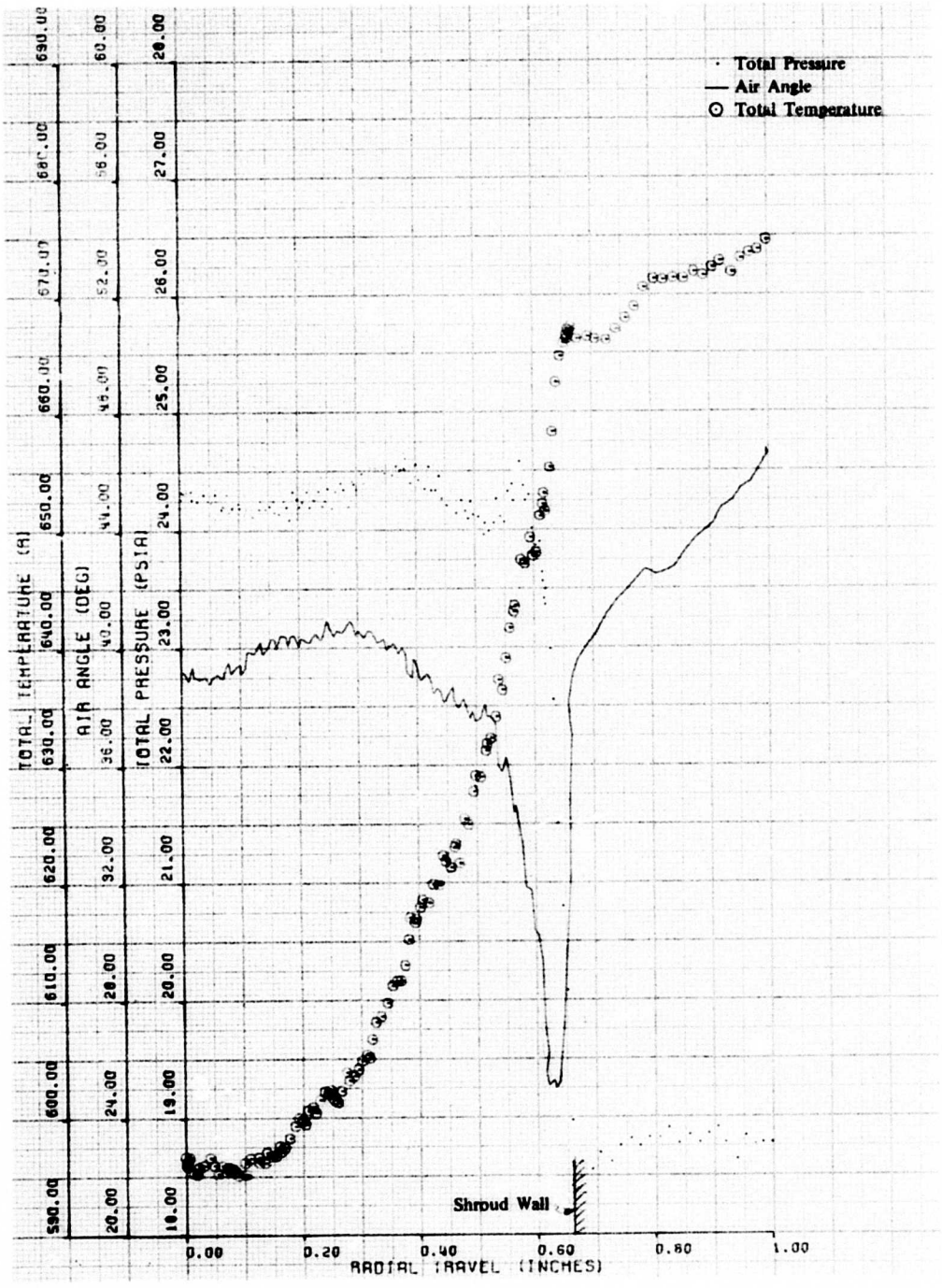

Figure A-8. Inducer Exit Traverse; 94% Speed, 15-deg IGV, Run 9.03.

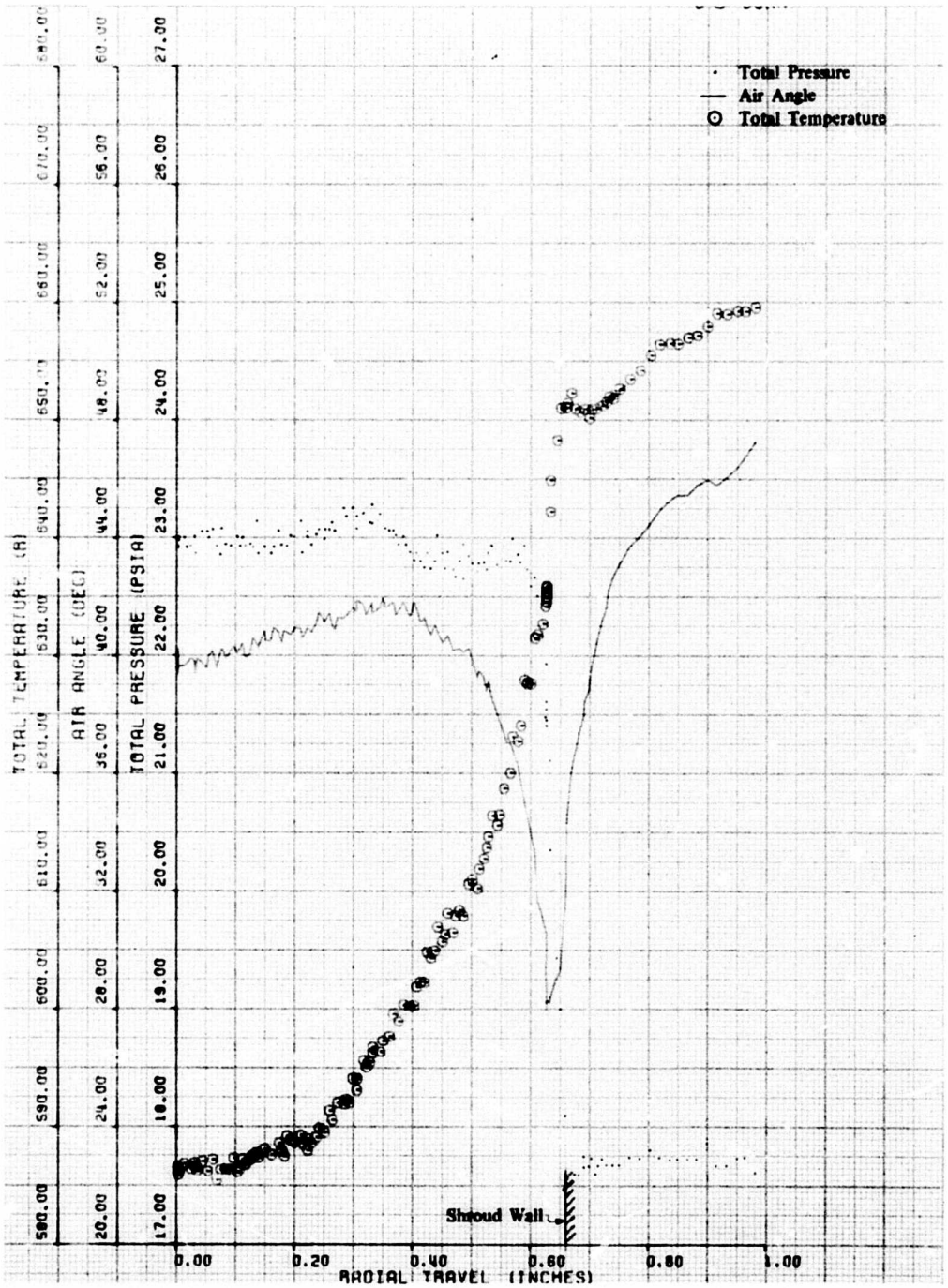

Figure A-9. Inducer Exit Traverse; 94% Speed, 20-deg IGV, Run 9.03.

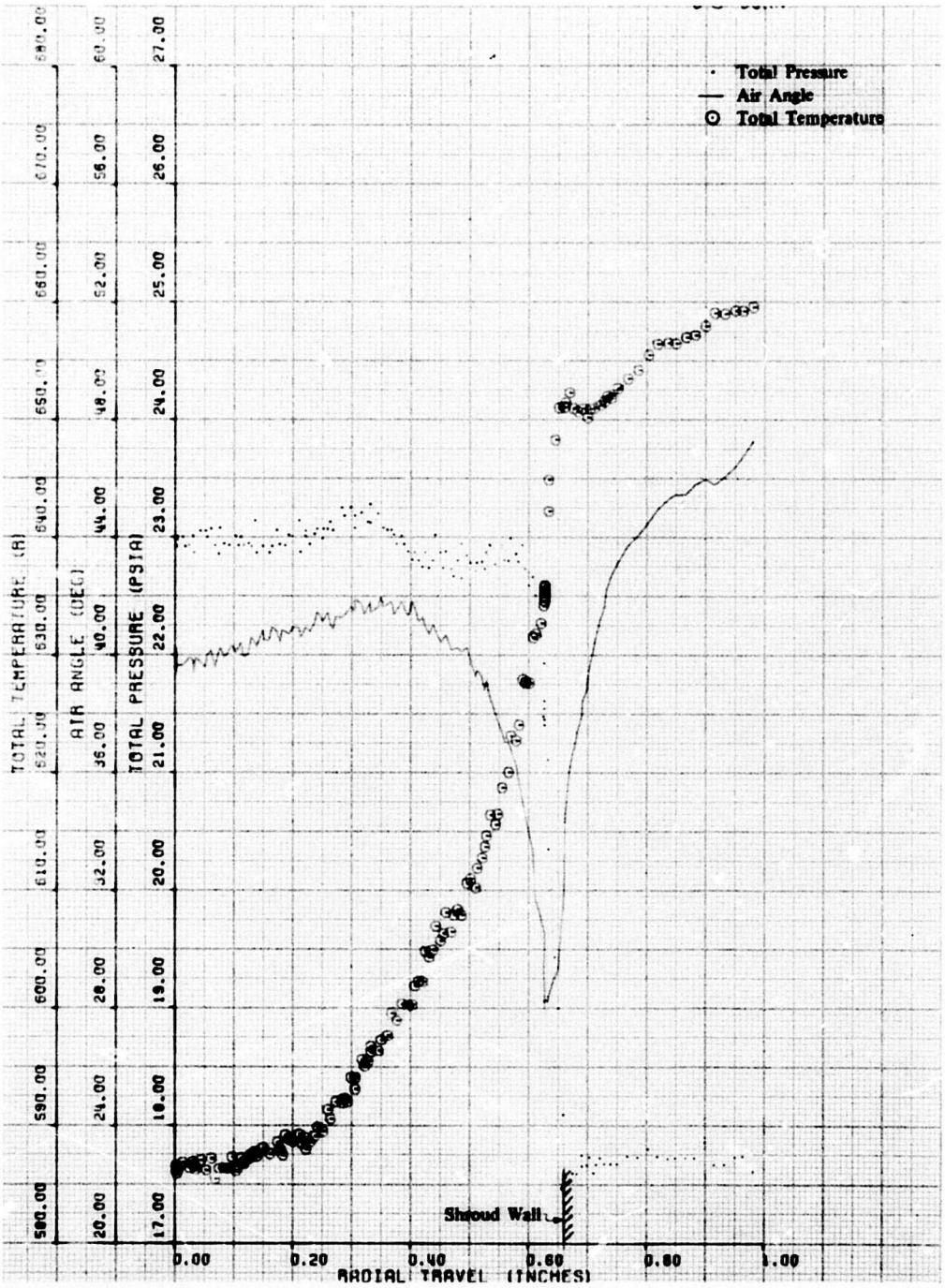

Figure A-9. Inducer Exit Traverse; 94% Speed, 20-deg IGV, Run 9.03.

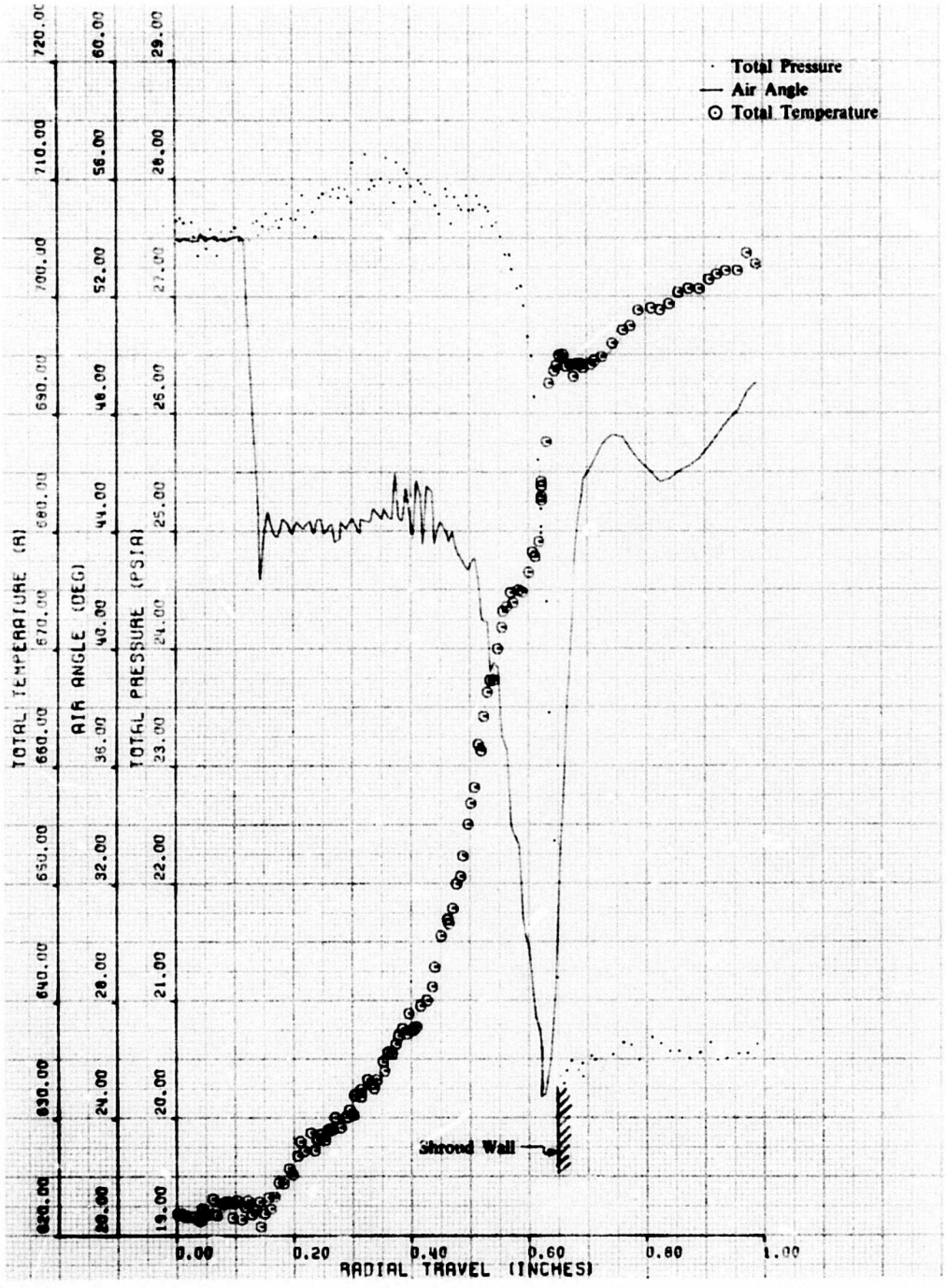

Figure A-10. Inducer Exit Traverse; 99% Speed, 0-deg IGV, Run 9.03.

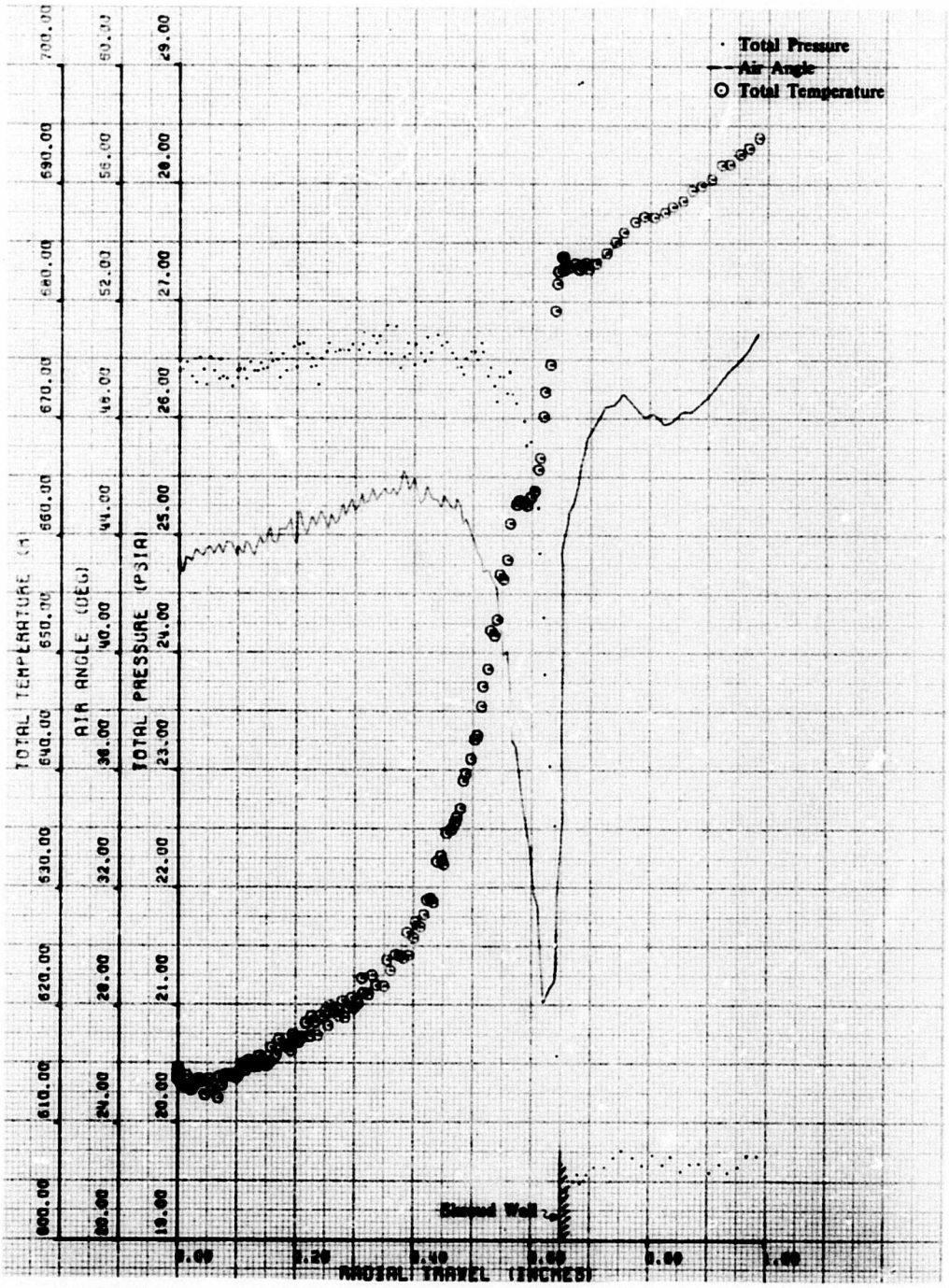

Figure A-11. Inducer Exit Traverse; 99.3% Speed, 5-deg IGV, Run 9.03.

LIST OF SYMBOLS

a	Speed of sound, ft/sec
A	Area, $in.^2$
A*	Critical area, $in.^2$
b	Chord, in.
C	Orifice equation constant
G	Gravitational constant = 32.174 lb_m-ft/lb_f-sec^2
E	Rotor frequency = $N_{act}/60$
e	Uncertainty of an individual sensor
h	Enthalpy/unit mass, Btu/lb_m
i	Incidence, deg = $\beta^* - \beta$
k	f (Mach No.) = $M\sqrt{\frac{\gamma G}{R}} \left(1 + \frac{\gamma-1}{2} M^2\right)^{-\frac{\gamma+1}{2(\gamma-1)}}$
K_1 & K_2	Orifice equation constants
LER	Leading-edge radius, in.
M	Absolute Mach number
n	Number of sensors
N	Rotor speed, rpm
P_s	Static pressure, psia
P_t	Total pressure, psia
PR	Pressure ratio
R_{le}	Diffuser leading-edge radius, in.
R_{tan}	Diffuser tangency radius, in.
R_{tip}	Impeller tip radius, in.
R	Gas constant = 53.345 ft-lb_f/lb_m-°R
t	Inducer blade maximum thickness, in.

T	Total temperature, °R
T_s	Static temperature, °R
TER	Trailing-edge radius, in.
TR	Temperature ratio
u	Overall uncertainty
U	Rotor speed, ft/sec
V	Absolute velocity, ft/sec
W	Weight flow, lb_m/sec
w	Relative velocity, ft/sec
α	Absolute air angle, deg from tangential direction
α_{CH}	Chord angle, deg from tangential direction
β	Relative air angle, deg from tangential direction
β^*	Leading-edge metal angle, deg from tangential direction
γ	Ratio of specific heats
δ	Pressure correction, $P_{t_0}/14.696$
Δ	Differential
η	Adiabatic efficiency
θ	Temperature correction, $\overline{T}_1/518.688$
θ^*	Camber, deg
τ	Gap between blades, in.
ϕ	Streamline angle, deg

Subscripts

0	Plenum
1	IGV exit
1.5	Inducer exit
2	Impeller exit

3	Collector
act	Actual
bl	Impeller bleed flow
cor	Corrected to standard day inlet conditions
F	Front
i	Index for local property of an increment
ind	Inducer
m	Streamline meridional component
net	Net (corrected for bleed effects)
T	Total
u	Tangential component

Superscripts

(-)	Mass averaged